DESY 97-112
June 1997

ISSN 0418-9833

A Search for Excited Fermions in e^+p Collisions at HERA

ZEUS Collaboration

hep-ex/9708007 5 Aug 1997

Abstract

Using the ZEUS detector at HERA, we have searched for heavy excited states of electrons, neutrinos, and quarks in e^+p collisions at a center-of-mass energy of 300 GeV. With an integrated luminosity of 9.4 pb^{-1}, no evidence was found for electroweak production and decay of such states. Limits on the production cross section times branching ratio and on the characteristic couplings, f/Λ, are derived for masses up to 250 GeV. For the particular choice $f/\Lambda = 1/M_{f^*}$, we exclude at the 95% confidence level excited electrons with mass between 30 and 200 GeV, excited electron neutrinos with mass between 40 and 96 GeV, and quarks excited electroweakly with mass between 40 and 169 GeV.

The ZEUS Collaboration

J. Breitweg, M. Derrick, D. Krakauer, S. Magill, D. Mikunas, B. Musgrave, J. Repond, R. Stanek, R.L. Talaga, R. Yoshida, H. Zhang
Argonne National Laboratory, Argonne, IL, USA [p]

M.C.K. Mattingly
Andrews University, Berrien Springs, MI, USA

F. Anselmo, P. Antonioli, G. Bari, M. Basile, L. Bellagamba, D. Boscherini, A. Bruni, G. Bruni, G. Cara Romeo, G. Castellini[1], L. Cifarelli[2], F. Cindolo, A. Contin, M. Corradi, S. De Pasquale, I. Gialas[3], P. Giusti, G. Iacobucci, G. Laurenti, G. Levi, A. Margotti, T. Massam, R. Nania, F. Palmonari, A. Pesci, A. Polini, F. Ricci, G. Sartorelli, Y. Zamora Garcia[4], A. Zichichi
University and INFN Bologna, Bologna, Italy [f]

C. Amelung, A. Bornheim, I. Brock, K. Coböken, J. Crittenden, R. Deffner, M. Eckert, L. Feld[5], M. Grothe, H. Hartmann, K. Heinloth, L. Heinz, E. Hilger, H.-P. Jakob, U.F. Katz, R. Kerger, E. Paul, M. Pfeiffer, Ch. Rembser, J. Stamm, R. Wedemeyer[6], H. Wieber
Physikalisches Institut der Universität Bonn, Bonn, Germany [c]

D.S. Bailey, S. Campbell-Robson, W.N. Cottingham, B. Foster, R. Hall-Wilton, M.E. Hayes, G.P. Heath, H.F. Heath, D. Piccioni, D.G. Roff, R.J. Tapper
H.H. Wills Physics Laboratory, University of Bristol, Bristol, U.K. [o]

M. Arneodo[7], R. Ayad, M. Capua, A. Garfagnini, L. Iannotti, M. Schioppa, G. Susinno
Calabria University, Physics Dept.and INFN, Cosenza, Italy [f]

J.Y. Kim, J.H. Lee, I.T. Lim, M.Y. Pac[8]
Chonnam National University, Kwangju, Korea [h]

A. Caldwell[9], N. Cartiglia, Z. Jing, W. Liu, B. Mellado, J.A. Parsons, S. Ritz[10], S. Sampson, F. Sciulli, P.B. Straub, Q. Zhu
Columbia University, Nevis Labs., Irvington on Hudson, N.Y., USA [q]

P. Borzemski, J. Chwastowski, A. Eskreys, Z. Jakubowski, M.B. Przybycień, M. Zachara, L. Zawiejski
Inst. of Nuclear Physics, Cracow, Poland [j]

L. Adamczyk[11], B. Bednarek, K. Jeleń, D. Kisielewska, T. Kowalski, M. Przybycień, E. Rulikowska-Zarębska, L. Suszycki, J. Zając
Faculty of Physics and Nuclear Techniques, Academy of Mining and Metallurgy, Cracow, Poland [j]

Z. Duliński, A. Kotański
Jagellonian Univ., Dept. of Physics, Cracow, Poland [k]

G. Abbiendi[12], L.A.T. Bauerdick, U. Behrens, H. Beier, J.K. Bienlein, G. Cases[13], O. Deppe, K. Desler, G. Drews, U. Fricke, D.J. Gilkinson, C. Glasman, P. Göttlicher, J. Große-Knetter, T. Haas, W. Hain, D. Hasell, K.F. Johnson[14], M. Kasemann, W. Koch, U. Kötz, H. Kowalski, J. Labs, L. Lindemann, B. Löhr, M. Löwe[15], O. Mańczak, J. Milewski, T. Monteiro[16], J.S.T. Ng[17], D. Notz, K. Ohrenberg[18], I.H. Park[19], A. Pellegrino, F. Pelucchi, K. Piotrzkowski, M. Roco[20], M. Rohde, J. Roldán, J.J. Ryan, A.A. Savin, U. Schneekloth, F. Selonke, B. Surrow, E. Tassi, T. Voß[21], D. Westphal, G. Wolf, U. Wollmer[22], C. Youngman, A.F. Żarnecki, W. Zeuner
Deutsches Elektronen-Synchrotron DESY, Hamburg, Germany

B.D. Burow, H.J. Grabosch, A. Meyer, S. Schlenstedt
DESY-IfH Zeuthen, Zeuthen, Germany

G. Barbagli, E. Gallo, P. Pelfer
University and INFN, Florence, Italy [f]

G. Maccarrone, L. Votano
INFN, Laboratori Nazionali di Frascati, Frascati, Italy [f]

A. Bamberger, S. Eisenhardt, P. Markun, T. Trefzger[23], S. Wölfle
Fakultät für Physik der Universität Freiburg i.Br., Freiburg i.Br., Germany [c]

J.T. Bromley, N.H. Brook, P.J. Bussey, A.T. Doyle, D.H. Saxon, L.E. Sinclair, E. Strickland, M.L. Utley[24], R. Waugh, A.S. Wilson
Dept. of Physics and Astronomy, University of Glasgow, Glasgow, U.K. [o]

I. Bohnet, N. Gendner, U. Holm, A. Meyer-Larsen, H. Salehi, K. Wick
Hamburg University, I. Institute of Exp. Physics, Hamburg, Germany [c]

L.K. Gladilin[25], D. Horstmann, D. Kçira, R. Klanner, E. Lohrmann, G. Poelz, W. Schott[26], F. Zetsche
Hamburg University, II. Institute of Exp. Physics, Hamburg, Germany [c]

T.C. Bacon, I. Butterworth, J.E. Cole, V.L. Harris, G. Howell, B.H.Y. Hung, L. Lamberti[27], K.R. Long, D.B. Miller, N. Pavel, A. Prinias[28], J.K. Sedgbeer, D. Sideris, A.F. Whitfield[29]
Imperial College London, High Energy Nuclear Physics Group, London, U.K. [o]

U. Mallik, S.M. Wang, J.T. Wu
University of Iowa, Physics and Astronomy Dept., Iowa City, USA [p]

P. Cloth, D. Filges
Forschungszentrum Jülich, Institut für Kernphysik, Jülich, Germany

J.I. Fleck[30], T. Ishii, M. Kuze, M. Nakao, K. Tokushuku, S. Yamada, Y. Yamazaki[31]
Institute of Particle and Nuclear Studies, KEK, Tsukuba, Japan [g]

S.H. An, S.B. Lee, S.W. Nam[32], H.S. Park, S.K. Park
Korea University, Seoul, Korea [h]

F. Barreiro, J.P. Fernández, G. García, R. Graciani, J.M. Hernández, L. Hervás[30], L. Labarga, M. Martínez, J. del Peso, J. Puga, J. Terrón, J.F. de Trocóniz
Univer. Autónoma Madrid, Depto de Física Teórica, Madrid, Spain [n]

F. Corriveau, D.S. Hanna, J. Hartmann, L.W. Hung, J.N. Lim, W.N. Murray, A. Ochs, M. Riveline, D.G. Stairs, M. St-Laurent, R. Ullmann
McGill University, Dept. of Physics, Montréal, Québec, Canada [a], [b]

T. Tsurugai
Meiji Gakuin University, Faculty of General Education, Yokohama, Japan

V. Bashkirov, B.A. Dolgoshein, A. Stifutkin
Moscow Engineering Physics Institute, Moscow, Russia [l]

G.L. Bashindzhagyan, P.F. Ermolov, Yu.A. Golubkov, L.A. Khein, N.A. Korotkova,
I.A. Korzhavina, V.A. Kuzmin, O.Yu. Lukina, A.S. Proskuryakov, L.M. Shcheglova,
A.V. Shumilin, A.N. Solomin, S.A. Zotkin
Moscow State University, Institute of Nuclear Physics, Moscow, Russia [m]

C. Bokel, M. Botje, N. Brümmer, F. Chlebana[20], J. Engelen, P. Kooijman, A. Kruse, A. van Sighem,
H. Tiecke, W. Verkerke, J. Vossebeld, M. Vreeswijk, L. Wiggers, E. de Wolf
NIKHEF and University of Amsterdam, Amsterdam, Netherlands [i]

D. Acosta, B. Bylsma, L.S. Durkin, J. Gilmore, C.M. Ginsburg, C.L. Kim, T.Y. Ling,
P. Nylander, T.A. Romanowski[33]
Ohio State University, Physics Department, Columbus, Ohio, USA [p]

H.E. Blaikley, R.J. Cashmore, A.M. Cooper-Sarkar, R.C.E. Devenish, J.K. Edmonds, N. Harnew,
M. Lancaster[34], J.D. McFall, C. Nath, V.A. Noyes[28], A. Quadt, O. Ruske, J.R. Tickner,
H. Uijterwaal, R. Walczak, D.S. Waters
Department of Physics, University of Oxford, Oxford, U.K. [o]

A. Bertolin, R. Brugnera, R. Carlin, F. Dal Corso, U. Dosselli, S. Limentani, M. Morandin,
M. Posocco, L. Stanco, R. Stroili, C. Voci
Dipartimento di Fisica dell' Universita and INFN, Padova, Italy [f]

J. Bulmahn, R.G. Feild[35], B.Y. Oh, J.R. Okrasiński, J.J. Whitmore
Pennsylvania State University, Dept. of Physics, University Park, PA, USA [q]

Y. Iga
Polytechnic University, Sagamihara, Japan [g]

G. D'Agostini, G. Marini, A. Nigro, M. Raso
Dipartimento di Fisica, Univ. 'La Sapienza' and INFN, Rome, Italy [f]

J.C. Hart, N.A. McCubbin, T.P. Shah
Rutherford Appleton Laboratory, Chilton, Didcot, Oxon, U.K. [o]

D. Epperson, C. Heusch, J.T. Rahn, H.F.-W. Sadrozinski, A. Seiden, D.C. Williams
University of California, Santa Cruz, CA, USA [p]

O. Schwarzer, A.H. Walenta
Fachbereich Physik der Universität-Gesamthochschule Siegen, Germany [c]

H. Abramowicz, G. Briskin, S. Dagan[36], T. Doeker, S. Kananov, A. Levy[37]
*Raymond and Beverly Sackler Faculty of Exact Sciences, School of Physics, Tel-Aviv University,
Tel-Aviv, Israel* [e]

T. Abe, T. Fusayasu, M. Inuzuka, K. Nagano, I. Suzuki, K. Umemori, T. Yamashita
Department of Physics, University of Tokyo, Tokyo, Japan [g]

R. Hamatsu, T. Hirose, K. Homma, S. Kitamura[38], T. Matsushita, K. Yamauchi
Tokyo Metropolitan University, Dept. of Physics, Tokyo, Japan [g]

R. Cirio, M. Costa, M.I. Ferrero, S. Maselli, V. Monaco, C. Peroni, M.C. Petrucci, R. Sacchi,
A. Solano, A. Staiano
Universita di Torino, Dipartimento di Fisica Sperimentale and INFN, Torino, Italy [f]

M. Dardo
II Faculty of Sciences, Torino University and INFN - Alessandria, Italy [f]

D.C. Bailey, M. Brkic, C.-P. Fagerstroem, G.F. Hartner, K.K. Joo, G.M. Levman, J.F. Martin, R.S. Orr, S. Polenz, C.R. Sampson, D. Simmons, R.J. Teuscher[30]
University of Toronto, Dept. of Physics, Toronto, Ont., Canada [a]

J.M. Butterworth, C.D. Catterall, T.W. Jones, P.B. Kaziewicz, J.B. Lane, R.L. Saunders, J. Shulman, M.R. Sutton
University College London, Physics and Astronomy Dept., London, U.K. [o]

B. Lu, L.W. Mo
Virginia Polytechnic Inst. and State University, Physics Dept., Blacksburg, VA, USA [q]

J. Ciborowski, G. Grzelak[39], M. Kasprzak, K. Muchorowski[40], R.J. Nowak, J.M. Pawlak, R. Pawlak, T. Tymieniecka, A.K. Wróblewski, J.A. Zakrzewski
Warsaw University, Institute of Experimental Physics, Warsaw, Poland [j]

M. Adamus
Institute for Nuclear Studies, Warsaw, Poland [j]

C. Coldewey, Y. Eisenberg[36], D. Hochman, U. Karshon[36], D. Revel[36]
Weizmann Institute, Nuclear Physics Dept., Rehovot, Israel [d]

W.F. Badgett, D. Chapin, R. Cross, S. Dasu, C. Foudas, R.J. Loveless, S. Mattingly, D.D. Reeder, W.H. Smith, A. Vaiciulis, M. Wodarczyk
University of Wisconsin, Dept. of Physics, Madison, WI, USA [p]

S. Bhadra, W.R. Frisken, M. Khakzad, W.B. Schmidke
York University, Dept. of Physics, North York, Ont., Canada [a]

[1] also at IROE Florence, Italy
[2] now at Univ. of Salerno and INFN Napoli, Italy
[3] now at Univ. of Crete, Greece
[4] supported by Worldlab, Lausanne, Switzerland
[5] now OPAL
[6] retired
[7] also at University of Torino and Alexander von Humboldt Fellow at University of Hamburg
[8] now at Dongshin University, Naju, Korea
[9] also at DESY
[10] Alfred P. Sloan Foundation Fellow
[11] supported by the Polish State Committee for Scientific Research, grant No. 2P03B14912
[12] supported by an EC fellowship number ERBFMBICT 950172
[13] now at SAP A.G., Walldorf
[14] visitor from Florida State University
[15] now at ALCATEL Mobile Communication GmbH, Stuttgart
[16] supported by European Community Program PRAXIS XXI
[17] now at DESY-Group FDET
[18] now at DESY Computer Center
[19] visitor from Kyungpook National University, Taegu, Korea, partially supported by DESY
[20] now at Fermi National Accelerator Laboratory (FNAL), Batavia, IL, USA
[21] now at NORCOM Infosystems, Hamburg
[22] now at Oxford University, supported by DAAD fellowship HSP II-AUFE III
[23] now at ATLAS Collaboration, Univ. of Munich
[24] now at Clinical Operational Research Unit, University College, London
[25] on leave from MSU, supported by the GIF, contract I-0444-176.07/95
[26] now a self-employed consultant
[27] supported by an EC fellowship
[28] PPARC Post-doctoral Fellow
[29] now at Conduit Communications Ltd., London, U.K.
[30] now at CERN
[31] supported by JSPS Postdoctoral Fellowships for Research Abroad
[32] now at Wayne State University, Detroit
[33] now at Department of Energy, Washington
[34] now at Lawrence Berkeley Laboratory, Berkeley, CA, USA
[35] now at Yale University, New Haven, CT
[36] supported by a MINERVA Fellowship
[37] partially supported by DESY
[38] present address: Tokyo Metropolitan College of Allied Medical Sciences, Tokyo 116, Japan
[39] supported by the Polish State Committee for Scientific Research, grant No. 2P03B09308
[40] supported by the Polish State Committee for Scientific Research, grant No. 2P03B09208

[a] supported by the Natural Sciences and Engineering Research Council of Canada (NSERC)
[b] supported by the FCAR of Québec, Canada
[c] supported by the German Federal Ministry for Education and Science, Research and Technology (BMBF), under contract numbers 057BN19P, 057FR19P, 057HH19P, 057HH29P, 057SI75I
[d] supported by the MINERVA Gesellschaft für Forschung GmbH, the German Israeli Foundation, and the U.S.-Israel Binational Science Foundation
[e] supported by the German Israeli Foundation, and by the Israel Science Foundation
[f] supported by the Italian National Institute for Nuclear Physics (INFN)
[g] supported by the Japanese Ministry of Education, Science and Culture (the Monbusho) and its grants for Scientific Research
[h] supported by the Korean Ministry of Education and Korea Science and Engineering Foundation
[i] supported by the Netherlands Foundation for Research on Matter (FOM)
[j] supported by the Polish State Committee for Scientific Research, grant No. 115/E-343/SPUB/P03/002/97, 2P03B10512, 2P03B10612, 2P03B14212, 2P03B10412
[k] supported by the Polish State Committee for Scientific Research (grant No. 2P03B08308) and Foundation for Polish-German Collaboration
[l] partially supported by the German Federal Ministry for Education and Science, Research and Technology (BMBF)
[m] supported by the German Federal Ministry for Education and Science, Research and Technology (BMBF), and the Fund of Fundamental Research of Russian Ministry of Science and Education and by INTAS-Grant No. 93-63
[n] supported by the Spanish Ministry of Education and Science through funds provided by CICYT
[o] supported by the Particle Physics and Astronomy Research Council
[p] supported by the US Department of Energy
[q] supported by the US National Science Foundation

1 Introduction

The existence of excited leptons or quarks would provide clear evidence for fermion substructure. Any theory of compositeness, however, would require a low energy limit which respects the symmetries of the Standard Model within the bounds provided by present experimental data. At the HERA electron-proton collider, single excited electrons (e^*) and quarks (q^*) could be produced by t-channel γ/Z^0 boson exchange, and excited neutrinos (ν^*) could be produced by t-channel W boson exchange. These mechanisms are depicted in Fig. 1.

We report on a search for resonances with masses above 30 GeV, produced in e^+p collisions at $\sqrt{s} = 300$ GeV, decaying to a light fermion through electroweak mechanisms. We interpret the results in the context of excited fermion (f^*) decays. The initial state positron implies that HERA would produce excited anti-leptons. To be succinct, the distinction between particles and anti-particles will be dropped in this paper. For example, "electron" will be used generically to refer to both e^- and e^+. The data sample, collected by ZEUS during the years 1994–1995, corresponds to an integrated luminosity of 9.4 pb^{-1}. This represents a 17-fold statistical increase over our previously published [1] limits from e^-p collisions. A search based on 2.75 pb^{-1} of e^+p data has been reported recently by the H1 Collaboration [2].

This paper is organized as follows. In the next section, we review the phenomenology of excited fermion production; in Section 3 we review the experimental constraints from direct searches at LEP and the Tevatron; and in Section 4 we describe the ZEUS detector, trigger configuration, and Monte Carlo simulations used to calculate acceptances and backgrounds. Section 5 describes the electron and photon identification criteria and the event kinematics determined from the calorimeter. Section 6 describes the selection criteria for the several f^* decay modes, followed in Section 7 by an estimate of the systematic uncertainties associated with these selections. In Section 8, we present the results on f^* production cross sections and couplings, and compare them with prior limits (an Appendix is included describing the details of our upper limit derivation). Finally, Section 9 summarizes the conclusions.

2 Excited Fermion Production Models

To maintain generality in describing f^* production and decay, without specifying the dynamics of the compositeness, it has been conventional to use the phenomenological Lagrangian of Hagiwara, Komamiya, and Zeppenfeld [3] describing the magnetic transitions between ordinary fermions (f) and spin $\frac{1}{2}$ excited states:

$$\mathcal{L}_{ff^*} \;=\; \frac{e}{\Lambda} \sum_{V=\gamma,Z,W} \overline{f}^* \, \sigma^{\mu\nu} \, (c_{Vf^*f} - d_{Vf^*f} \, \gamma^5 \,) \, f \, \partial_\mu V_\nu \;+\; h.c. \qquad (1)$$

Here Λ is the compositeness scale, and c_{Vf^*f} and d_{Vf^*f} are coupling constants at the $f \leftrightarrow f^*$ transition vertex, labelled for each vector boson, V. Excitations of spin $\frac{3}{2}$ excited states, which involve a larger number of arbitrary parameters, are discussed in Ref. [4] but will not be considered here.

The agreement between the precise measurements of electron/muon $g-2$ and theoretical predictions implies that $|c_{\gamma f^* f}| = |d_{\gamma f^* f}|$ for compositeness scales less than 10–100 TeV [5]. The absence of electron and muon electric dipole moments forces $c_{\gamma f^* f}$ and $d_{\gamma f^* f}$ to have the same phase. It is customary to choose a model [3] which couples left-handed fermions to right-handed excited states, and in which the excited fermions form both left- and right-handed weak isodoublets. The interaction Lagrangian, including excited leptons and quarks [6, 7], can be written:

$$\mathcal{L}_{f f^*} \;=\; \frac{1}{\Lambda}\,\overline{f^*}_{\rm R}\;\sigma^{\mu\nu}\;\left[g f\frac{\tau^{\rm a}}{2}\mathbf{W}^{\rm a}_{\mu\nu} + g' f'\frac{Y}{2}B_{\mu\nu} + g_{\rm s} f_{\rm s}\frac{\lambda^{\rm a}}{2}\mathbf{G}^{\rm a}_{\mu\nu}\right]\;f_{\rm L}\;\; + h.c. \tag{2}$$

where $\mathbf{W}^{\rm a}_{\mu\nu}$, $B_{\mu\nu}$, and $\mathbf{G}^{\rm a}_{\mu\nu}$ are the field-strength tensors of the $SU(2)_L$, $U(1)_Y$, and $SU(3)_C$ gauge fields respectively; $\tau^{\rm a}$, Y, and $\lambda^{\rm a}$ are the corresponding gauge group generators; and g, g', and $g_{\rm s}$ are the corresponding gauge coupling constants. The unknown parameters f, f', and $f_{\rm s}$ depend on the specific dynamics describing the compositeness. The electroweak coupling constants of Eq. (1), with $c_{V f^* f} = d_{V f^* f}$, may be expressed[1]:

$$\begin{aligned} c_{\gamma f^* f} &= \frac{1}{2}(f\,T_3 + f'\,\frac{Y}{2}) \\ c_{Z f^* f} &= \frac{1}{2}(f\,T_3\cot\theta_{\rm W} - f'\,\frac{Y}{2}\tan\theta_{\rm W}) \\ c_{W f^* f} &= \frac{f}{2\sqrt{2}\sin\theta_{\rm W}} \end{aligned} \tag{3}$$

where T_3 is the third component of the weak isospin, Y is the weak hypercharge (-1 for leptons and $\frac{1}{3}$ for quarks), and $\theta_{\rm W}$ is the weak mixing angle. For specific assumptions relating f, f', and $f_{\rm s}$, the branching fractions are known. Additionally, the cross sections are described by a single parameter (e.g., f/Λ) with dimension, GeV^{-1}.

The cross section for f^* production in $e\,p$ collisions has been calculated [3, 7]. For excited electron ($f^* = e^*$) production, t-channel γ exchange (Fig. 1a) is expected to dominate, with the elastic contribution ($X = p$) approximately 50% of the cross section. Production of excited neutrinos ($\nu^*_{\rm e}$) proceeds via W exchange (Fig. 1b), for which the negative square of the four-momentum transferred by the exchanged boson (Q^2) is large, the cross section is small, and there is no elastic channel. We also searched for excited quarks (q^*) produced through electroweak couplings illustrated in Fig. 1c. This is complementary to q^* searches at hadron colliders.

For the presumed large f^* masses involved in all these searches, a substantial fraction of the available center-of-mass energy is required to provide the mass, M_{f^*}. HERA kinematics forces any f^* with mass larger than twice the electron beam energy to be boosted in the proton beam direction with little transverse momentum. The decay products of the f^*, on the other hand, typically have large laboratory angles and large transverse momenta.

Produced f^* decay to a light fermion and a gauge boson. The partial electroweak decay

[1] These definitions for f, f', and $f_{\rm s}$ differ by a factor of 2 from the convention used in Refs. [6] and [7]

.

widths for $f^* \to f\,V$ (with $V = \gamma$, Z^0, or W) are given by [7]

$$\Gamma(f^* \to fV) \;=\; \alpha\,\frac{M_{f^*}^3}{\Lambda^2}\,c_{Vf^*f}^2\left(1-\frac{M_V^2}{M_{f^*}^2}\right)^2\left(1+\frac{M_V^2}{2M_{f^*}^2}\right) \tag{4}$$

for the vector boson mass $M_V < M_{f^*}$. As is conventional, we choose $f = f'$ in interpreting our search for e^* decay (for $M_{f^*} \gg M_V$, the W decay mode for excited electrons dominates with this choice). The decay $\nu_{\rm e}^* \to \nu_{\rm e}\,\gamma$ is forbidden unless $f \neq f'$. We choose $f = -f'$ in the interpretation of our search for $\nu_{\rm e}^*$ decays. The partial width for q^* decaying with gluon emission is obtained from (4) by replacing the electroweak coupling, α, with $\frac{4}{3}\alpha_{\rm s}$, where $\alpha_{\rm s}$ is the quark-gluon coupling. For the assumption that $f_{\rm s}$ is comparable in magnitude to f and f', the decay of excited quarks into gluons dominates all other decays since $\alpha_{\rm s}$ is so much larger than α. As discussed in Section 3, Tevatron experiments limit $f_{\rm s}$, whereas for small $f_{\rm s}$, the high mass electroweak limits provided here on f and f' are unique. For values of M_{f^*} considered in this paper, the total electroweak decay width is approximately 1 GeV or less.

3 Direct Limits from $e^+\,e^-$ and $\overline{p}\,p$ Colliders

Excited leptons and quarks also might be directly produced in e^+e^- and $\overline{p}p$ collisions. LEP searches at $\sqrt{s}$ = 130–140 GeV [8] and at $\sqrt{s}$ = 161 GeV [9] rule out at the 95% confidence level any excited lepton ($e^*, \mu^*, \tau^*, \nu^*$) with mass below approximately 80 GeV. Since such excited fermions would be pair produced, these limits are independent of the coupling parameters f and f'. Single excited leptons also can be produced at LEP in a manner analogous to that at HERA: each of the four experiments set upper limits at the 95% confidence level on f/Λ (assuming $f = f'$) at the level of (0.3–1.0)$\times 10^{-3}$ GeV^{-1} for excited electrons and $\mathcal{O}(10^{-2})$ GeV^{-1} for all other lepton species with masses up to nearly the LEP center-of-mass energy. The larger center-of-mass energy at HERA allows for sensitivity at higher masses.

The CDF experiment has searched for excited quarks produced in $\overline{p}\,p$ collisions at $\sqrt{s}$ = 1800 GeV. Initially, only decay modes where the excited quark decays to a quark and photon or to a quark and W boson decaying leptonically [10] were considered. Limits were set at the 95% confidence level on excited quarks in the mass range 80–540 GeV under the assumptions $f = f' = f_{\rm s} = \frac{1}{2}$ (their convention differs by a factor two from ours) and $\Lambda = M_{q^*}$. More recently, the same group has looked for evidence in high transverse energy jet samples of a resonance characteristic of excited quarks decaying through gluon couplings [11], so that visible signatures require only $f_s \neq 0$. No evidence of a resonance was seen, permitting extension of the upper limit under the above assumptions to 760 GeV, except for a window between 570 and 580 GeV. These results translate to an upper limit on $f_{\rm s}/\Lambda$ of (0.5–1.0)$\times 10^{-3}$ GeV^{-1} for the given mass range under the stated assumptions.

It should be noted that searches for excited quarks at HERA are complementary to those at hadron colliders. All Tevatron limits assume coupling through the gluon ($f_s \neq 0$) whereas HERA limits on electroweak couplings f and f' are strongest for $f_s = 0$.

4 Experimental Setup and Event Simulation

The data used in this analysis were collected with the ZEUS detector. The HERA beam energies were 27.5 GeV for positrons and 820 GeV for protons.

4.1 The ZEUS Detector

ZEUS is a nearly hermetic, multipurpose, magnetic detector described in detail elsewhere [12, 13]. The primary components used in this analysis are the high resolution depleted-uranium scintillator calorimeter, the central tracking detectors, and the luminosity detector.

The ZEUS coordinate system is right-handed with the Z axis pointing in the proton beam direction, referred to as the "forward" direction. The X axis points horizontally toward the center of HERA, and the origin is at the nominal interaction point. The polar angle θ is measured with respect to the Z direction, and the corresponding pseudorapidity is $\eta = -\ln\tan(\theta/2)$.

The compensating calorimeter [14] consists of three parts: the forward calorimeter (FCAL) covering $2.6^\circ < \theta < 36.7^\circ$, the barrel calorimeter (BCAL) covering $36.7^\circ < \theta < 129.1^\circ$, and the rear calorimeter (RCAL) covering $129.1^\circ < \theta < 176.2^\circ$. Each part of the calorimeter is subdivided longitudinally into one electromagnetic section (EMC), and one or two hadronic sections (HAC) for the RCAL or FCAL/BCAL, respectively. Each section is further subdivided transversely into cells of 5×20 cm^2 (10×20 cm^2 in RCAL) for the EMC sections and 20×20 cm^2 for the HAC sections. The calorimeter has an energy resolution of $\sigma_E/E = 0.18/\sqrt{E(\mathrm{GeV})}$ for electrons and $\sigma_E/E = 0.35/\sqrt{E(\mathrm{GeV})}$ for hadrons as measured under test beam conditions. The cell-to-cell variations in the energy calibration are approximately 2% for the EMC cells and 3% for HAC cells. The FCAL and BCAL energy scale calibrations are presently known to 3%. The calorimeter provides time measurements with resolution better than 1 ns for energy deposits above 4.5 GeV.

The tracking components used in this analysis are the vertex detector [15] and the central tracking detector [16], operating in a 1.43 T solenoidal magnetic field. The central tracking detector is capable of reconstructing the tracks over the region $15^\circ < \theta < 165^\circ$ and also supplies a vertex measurement for each event. The transverse momentum resolution for tracks intersecting all tracking layers is $\sigma(p_\mathrm{t})/p_\mathrm{t} = [0.005\, p_\mathrm{t}(\mathrm{GeV})] \oplus 0.016$.

The luminosity was measured to a precision of about 1.5% from the rate of energetic bremsstrahlung photons produced in the process $e\,p \to e\,p\,\gamma$. The photons are detected in a lead-scintillator calorimeter [17] placed at $Z = -107$ m.

4.2 Trigger Configuration

Events were filtered online by a three-level trigger system [13]. The trigger criteria used in this analysis relied primarily on the energies measured in the calorimeter. The trigger decision was based on electromagnetic energy, total transverse energy (E_t), missing

transverse momentum ($\not{P}_{\rm t}$), $E - P_{\rm Z}$, and timing. Thresholds on kinematic parameters, in general, were significantly below the corresponding offline cuts described in Section 6.

4.3 Monte Carlo Simulation

The acceptance due to our selection criteria is calculated with a Monte Carlo simulation of excited fermion production and decay. This analysis uses the code HEXF [18], based on the models discussed earlier [3, 6, 7]. Interference with Standard Model processes is not considered. Initial state radiation from the beam electron uses the Weizsäcker-Williams approximation [19]. The hadronic final state is simulated using the matrix element and parton shower approach of LEPTO [20] for the hard QCD parton cascade, and JETSET [21] for the soft hadronization. The MRSA[22] parton distribution set is used for inelastic scattering.

A particular choice of parameters must be made in the excited fermion production model in order to determine the detector acceptance. We have adopted the convention $f = f'$ in the Lagrangian[2] (2), except for the decay $\nu_{\rm e}^* \to \nu_{\rm e}\,\gamma$ where we choose $f' = -f$ to achieve a non-zero coupling (note that the production cross section depends only on f, however). The acceptance only weakly depends on these assumptions.

Backgrounds from charged and neutral current Deep Inelastic Scattering (DIS) are simulated using HERACLES [23], including first-order electroweak radiative corrections. The hadronic final states use LEPTO and JETSET interfaced to HERACLES using DJANGO [24]. Resolved and direct photoproduction backgrounds, including prompt photon production, are simulated with the HERWIG generator [25]. QED-Compton scattering events are generated with COMPTON [26]. Finally, production of W bosons, a potential background to rare topologies, uses the EPVEC generator [27].

All simulated events are passed through a detector simulation based on GEANT [28], incorporating our knowledge of the detector and trigger, and subsequently processed by the same reconstruction and analysis programs used for data.

5 Electromagnetic Cluster Identification and Event Kinematics

Excited fermions decaying to electrons or photons give rise to isolated electromagnetic (EM) clusters in the calorimeter, identified by the characteristically small longitudinal and lateral profiles. Pattern recognition combines a neural network algorithm [29] and a requirement limiting the shower width along the direction of the 5 cm cell segmentation in the BCAL and FCAL (no cut is applied in the RCAL). The shower widths are required to be less than 4 cm (5 cm) in the BCAL (FCAL).

EM clusters are said to be *isolated* if they satisfy a criterion based on the sum of the transverse energy, E_R, within a cone of radius $R = \sqrt{(\Delta\eta)^2 + (\Delta\phi)^2}$ centered on the

[2] The value of f_s is only relevant for the q^* search, where we describe the assumptions more fully.

cluster, contributed by all calorimeter cells *unassociated* with the EM cluster. Depending on the desired degree of isolation, the choice for R is either 0.7 or 1.5, and the requirement is $E_R < 2$ GeV.

The event selection for the excited fermion searches requires the following global event quantities calculated from the event vertex and the calorimeter cell measurements:

$$\begin{aligned} E - P_{\rm Z} &= \sum_{\rm i} \left(E_{\rm i} - P_{\rm Z,i}\right) \\ E_{\rm t} &= \sum_{\rm i}{}' \sqrt{P_{\rm X,i}^2 + P_{\rm Y,i}^2} \\ \not{P}_{\rm t} &= \sqrt{\left(\textstyle\sum_{\rm i} P_{\rm X,i}\right)^2 + \left(\textstyle\sum_{\rm i} P_{\rm Y,i}\right)^2} \\ M &= \sqrt{\left(\textstyle\sum_{\rm i}{}' E_{\rm i}\right)^2 - \left(\textstyle\sum_{\rm i}{}' P_{\rm X,i}\right)^2 - \left(\textstyle\sum_{\rm i}{}' P_{\rm Y,i}\right)^2 - \left(\textstyle\sum_{\rm i}{}' P_{\rm Z,i}\right)^2} \end{aligned} \tag{5}$$

where $E_i = \sqrt{P_{\rm X,i}^2 + P_{\rm Y,i}^2 + P_{\rm Z,i}^2}$ is the energy in the ith calorimeter cell.

$E_{\rm t}$ is the total scalar sum of the transverse energy deposited in the calorimeter, $\not{P}_{\rm t}$ is the missing transverse momentum, and M is the measured mass. Momentum conservation dictates that the longitudinal momentum variable, $E - P_{\rm Z}$, equals twice the incident electron beam energy ($2E_e = 55$ GeV) for final states in which no energy escapes through the rear beam hole.

The unprimed sums run over all calorimeter cells with energy deposits above a set threshold. The primed sums (in the calculations of $E_{\rm t}$ and M) exclude the cells in the forward cone, $\theta < 10^\circ$ (this reduces sensitivity to particles within the proton remnant). Any of these quantities with the subscript "had" also exclude cells in the calorimeter sum (double primed sum) which belong to clusters which are identified as candidate electrons or photons from f^* decay. For example, the azimuthal ($\phi_{\rm had}$) and polar ($\theta_{\rm had}$) angles respectively for the hadronic system are defined:

$$\begin{aligned} \phi_{\rm had} &= \arctan \frac{\sum_{\rm i}{}'' P_{\rm Y,i}}{\sum_{\rm i}{}'' P_{\rm X,i}} \\ \theta_{\rm had} &= \arccos \frac{\sum_{\rm i}{}'' P_{\rm Z,i}}{\sqrt{\left(\sum_{\rm i}{}'' P_{\rm X,i}\right)^2 + \left(\sum_{\rm i}{}'' P_{\rm Y,i}\right)^2 + \left(\sum_{\rm i}{}'' P_{\rm Z,i}\right)^2}}. \end{aligned} \tag{6}$$

6 Event Selection

The processes of interest for production of the various f^* are

$$\begin{aligned} e + p &\to e^* + X \\ e + p &\to \nu^* + X \end{aligned} \tag{7}$$

for excited leptons, and

$$e + p \to e + q^* + X \tag{8}$$

for excited quarks. Here X represents the proton remnant (or proton in the case of elastic e^* production). An important feature of these processes is that reactions (7) involve an

excited lepton which subsequently decays into at least one high transverse momentum lepton. Reaction (8), by contrast, involves a final state excited quark *and* a final state electron. This electron typically travels in the direction of the electron beam and has low transverse momentum.

The searches are organized in this section by event topology. We have sought the following excited fermion decays:

1. $e^* \to e\,\gamma$
2. $e^* \to e\,Z^0 \to e\,q\,\overline{q}$ and $\nu_{\rm e}^* \to e\,W \to e\,q\,\overline{q}$
3. $e^* \to \nu_{\rm e}\,W \to \nu_{\rm e}\,q\,\overline{q}$ and $\nu_{\rm e}^* \to \nu_{\rm e}\,Z^0 \to \nu_{\rm e}\,q\,\overline{q}$
4. $\nu_{\rm e}^* \to \nu_{\rm e}\,\gamma$
5. $e^* \to e\,Z^0 \to e\,\nu\,\overline{\nu}$ and $e^* \to \nu_{\rm e}\,W \to e\,\nu_{\rm e}\,\overline{\nu}_{\rm e}$
6. $\nu_{\rm e}^* \to e\,W \to e\,\overline{e}\,\nu_{\rm e}$
7. $q^* \to q\,\gamma$
8. $q^* \to q\,W \to q\,\overline{e}\,\nu_{\rm e}$

The conclusions for each f^* are discussed in Section 8 and summarized in Tab. 1. Also shown in this table are the decay signature, typical acceptance, number of observed events, and number of expected events from background sources for each f^* decay mode described above.

The following selection cuts, common to all channels, were applied to ensure that the selected events are $e\,p$ interactions.

1. Events are required to have a reconstructed vertex measured by the central tracking detectors, and it must lie within 50 cm of the nominal collision point along the Z axis.[3]
2. The arrival times measured with the calorimeter are required to be consistent with final state particles originating from the nominal collision point.
3. Pattern recognition algorithms are applied to suppress non-$e\,p$ backgrounds (cosmic rays, beam halo muons, p–gas interactions, and photomultiplier sparks). In addition, each final event sample is visually inspected, and a few remaining events are removed which fall into one of these background categories.

In addition, since the decay products of heavy leptons would be forward-going, the total calorimeter energy, $E_{\rm rear}$, deposited in the cone $\theta > 150°$ is required to be less than 2 GeV. As discussed in Section 6.7, this cut is different for excited quark searches as a scattered electron may be detected in the rear direction.

[3]The Z vertex distribution is approximately Gaussian with an r.m.s. spread of 12 cm, a consequence of the proton bunch length.

6.1 $e\,\gamma$ Resonance Search

The signature for the decay $e^* \to e\,\gamma$ is the observation in the calorimeter of two isolated EM clusters. QED-Compton scattering ($e\,p \to e\,\gamma\,X$) has a similar topology, and thus forms a non-resonant background at predominantly low electron-photon masses, $M_{e\gamma}$. The angular distribution is different [3], however, so the two may be statistically separated. Additional backgrounds arise from neutral current DIS events with an isolated π^0. Two-photon production of electron pairs also produces two electromagnetic showers, albeit with tracks, but is found to be negligible.

The following selections are required:

1. Each EM cluster is required to have a transverse energy larger than 10 GeV, and each cluster must be isolated from hadronic activity by an η–ϕ cone radius $R = 0.7$ (see Section 5). We do not require a track to be associated with either EM cluster.

2. Low Q^2 DIS events with a π^0 in the forward region are suppressed by requiring that the polar angle of each EM cluster be larger than 15°, or that each EM cluster energy be larger than 32 GeV (the polar angle cut alone would severely limit the acceptance for high mass excited electrons).

3. The net $E - P_{\rm Z}$ of the two electromagnetic clusters must reflect longitudinal momentum conservation, so it is required to be in the range 35 to 65 GeV. This limits any vertex mismeasurement as well as initial state radiation.

4. The transverse energy deposited in the calorimeter by the two clusters must account for more than 70% of the total transverse energy. This reduces neutral current DIS background.

5. Events with more than three well-measured tracks in the central tracking detector[4] are rejected. This preferentially selects elastic e^* production.

The selection criteria accept e^* produced with momentum transfers as large as $Q^2 \approx 1000$ GeV^2, and so includes a large fraction of the expected production (with $f = f'$).[5] The acceptance varies from 40% at $M_{e\gamma} = 30$ GeV to 80% for $M_{e\gamma} > 150$ GeV. The background from neutral current DIS is estimated to be 16.0 ± 2.4 events, and the background from QED-Compton scattering is estimated to be 81.5 ± 4.1 events. The sum agrees well with the 103 events selected from data.

The electron-photon invariant mass, $M_{e\gamma}$, is determined using the polar angles, θ_e and θ_γ, of the e and γ clusters, respectively. The formula assumes that the recoiling hadron

[4]Such tracks must have transverse momentum $P_{\rm t} > 0.2$ GeV and $15° < \theta < 165°$.

[5]The model of Ref. [3] (with $f = f'$) predicts that e^* are preferentially produced at low Q^2; approximately 60% are produced elastically or quasi-elastically. Only for $f' \approx -f$ in Eq. (3) is the coupling to photons suppressed and the coupling to the Z^0 dominant. In this case, the total e^* production would be much smaller, and a large fraction would have $Q^2 > 1000$ GeV^2, which would be rejected by the selection criteria. However, even for $f' = -0.75f$, 35% of all excited electrons are produced with $Q^2 < 5$ GeV^2.

system has negligible transverse momentum and that $E - P_Z = 2E_e$ for the $e\,\gamma$ pair:

$$M^2_{e\gamma} \;=\; (2E_e)^2\,\frac{\sin\theta_\gamma + \sin\theta_e + \sin(\theta_\gamma + \theta_e)}{\sin\theta_\gamma + \sin\theta_e - \sin(\theta_\gamma + \theta_e)} \tag{9}$$

Here E_e is the electron beam energy. This formula provides a mass resolution for elastically produced excited electrons nearly a factor of 5 better than that obtained from the measured four-momentum in the calorimeter. It also reduces the sensitivity to systematic uncertainty in the calorimeter energy scale. However, no improvement in the resolution is obtained for inelastically produced e^* because the recoiling hadron system has been ignored. Non-radiative low Q^2 events tend to occupy the central portion of an e^* peak, while events with initial state radiation would produce a high energy tail in an e^* mass peak. It follows that the formula (9), together with the selections, introduces some model dependence in the acceptance. Nevertheless, low Q^2 events are predicted to dominate the rate for essentially any non-zero coupling to the photon (which must be the case for the $e\gamma$ final state to occur). Hence, if $e^* \to e\,\gamma$ were detected, a narrow central peak in the $M_{e\gamma}$ distribution derived from (9) is expected. The unshaded histogram in Fig. 2 shows the expected lineshape for an excited electron of mass 150 GeV. The mass resolution determined from a Gaussian fit to the central region of the Monte Carlo lineshape varies from 0.5 GeV at a mass of 50 GeV to 1.8 GeV at a mass of 200 GeV.

Figure 2 shows the invariant mass spectrum obtained for data (solid points) compared with the Monte Carlo predicted background (shaded histogram). The Kolmogorov test [30] applied to the mass distribution, which assigns a probability to the spectrum *shape*, yields a probability of 23% that the observed distribution comes from background. Four events are found to cluster at a mass of 135 GeV, which is significant given the small expected background (2.5 events with $M_{e\gamma} > 100$ GeV). However, a resonance at $M_{e\gamma}$ should exhibit a Jacobian peak at $M_{e\gamma}/2$ in the distribution of the transverse energy of each shower. Instead, three of the four events have shower transverse energies less than 32 GeV, at the tail of the expected distribution. These three events also exhibit some hadronic energy around the photon candidate, and the EM clusters are near the minimum energy or angle requirements. The features of these three events are consistent with neutral current DIS background. The fourth event, with an average shower transverse energy of 54 GeV, has no hadronic energy, but both EM clusters have matching tracks. It is consistent with an event in which the photon converts near the vertex. We conclude that the data are consistent with background expectations.

6.2 $e\,q\,\overline{q}$ Resonance Search

The $e\,q\,\overline{q}$ final state could arise from $e^* \to e\,Z^0$ or $\nu_e^* \to e\,W$ decays in which the Z^0 or W decays hadronically (additional Z^0 and W decay modes are described in Sections 6.5 and 6.6). The search makes use of (a) selections to obtain events with the characteristics expected for this decay mode; and (b) calculation of the final state mass (M_{eZ} or M_{eW}). No distinction is made between excited electrons and excited neutrinos for purposes of optimizing cuts and calculating backgrounds in this search, since both involve a topology with a high energy electron and two jets. With ν_e^* production proceeding through W exchange, the characteristic Q^2 of the exchanged boson is typically much larger than for

e^* production. The only difference in the final state topology aside from the $q\,\overline{q}$ mass, therefore, involves the elasticity of the final state hadronic system associated with the struck proton. The dominant background to this search arises from multi-jet neutral current DIS. Global event variables (without explicit jet algorithms) are used to separate the signal from this background.

For this search, an EM cluster with transverse energy larger than 15 GeV must be identified with $\theta < 115°$. The shower isolation requirement (see Section 5) is dropped because the electron from an f^* decay is often near some hadronic activity when produced near threshold. The measured longitudinal momentum variable, $E - P_{\rm Z}$, must be in the range 35 to 65 GeV. Large hadronic transverse energy ($E_{\rm t,had}$) and large invariant mass ($M_{\rm had}$), discussed in Section 5, must be measured from the calorimeter. Specifically, either $E_{\rm t,had} > 60$ GeV and $M_{\rm had} > 60$ GeV, or $E_{\rm t,had} > 70$ GeV and $M_{\rm had} > 40$ GeV is required. The latter selection provides good acceptance for high mass f^* decays in which hadrons from the decay of the heavy boson are often lost in the very forward region. Remaining cosmic ray backgrounds are suppressed by requiring approximate momentum balance in the transverse plane: $\not{P}_{\rm t}/E_{\rm t} < 0.15$.

The electron-boson invariant mass, M_{eV}, is calculated from the energy and angle of the decay electron because it is more accurate than the invariant mass calculated from the entire calorimeter, which suffers from leakage in the very forward region and the poorer hadronic energy resolution. The formula, derived assuming the f^* has negligible transverse momentum and $E - P_{\rm Z} = 2E_e$, is

$$M_{eV}^2 \;=\; \frac{4E_e E_e' \cos^2\frac{\theta_e}{2} + M_V^2}{1 - E_e'/E_e \sin^2\frac{\theta_e}{2}} \qquad (10)$$

where E_e is the electron beam energy, E_e' is the decay electron energy, θ_e is the polar angle of the decay electron, and M_V is the mass of the gauge boson. The mass resolution, determined from Monte Carlo simulations, is approximately 6 GeV for excited electrons and 18 GeV for excited neutrinos, the latter being larger because the underlying assumptions of Eq. (10) are not rigorously correct when Q^2 is large. The unshaded histogram in Fig. 3 shows the expected lineshape for an e^* of mass 225 GeV.

The ratio of the total calorimeter invariant mass (Eq. 5), M, to the mass derived in Eq. (10) is used to further reject backgrounds. Approximately one-third of the remaining background is removed when the cut $M/M_{eZ} > 0.82$ is applied.

Above threshold the acceptance for the $e\,q\,\overline{q}$ final state is approximately 55% for e^* production, and 70% for $\nu_{\rm e}^*$ production. The total number of selected events is 21, compared with a background expectation of 15.3 ± 1.5. The distribution in M_{eZ} for the selected events with the $e^* \to e\,Z^0$ hypothesis is shown in Fig. 3 for data (solid points) compared with the Monte Carlo background (shaded histogram). No significant excess is observed. The Kolmogorov test applied to the mass distribution yields a probability of 86% that the shape of the observed distribution is consistent with the expected background.

6.3 $\nu_e\, q\, \overline{q}$ Resonance Search

The $\nu_e\, q\, \overline{q}$ final state would arise from $e^* \to \nu_e W$ or $\nu^* \to \nu_e Z^0$ decays where the Z^0 or W decays hadronically (an additional W decay mode is $e^* \to \nu_e W \to e\, \nu_e \overline{\nu}_e$, described in Section 6.5). The technique, using event topology and invariant mass, is similar to that in Section 6.2. Again the same selection is used for the excited electron and excited neutrino searches. The dominant background consists of multi-jet charged current DIS events.

The presence of a neutrino is inferred from substantial missing momentum measured in the calorimeter: $\not{P}_t > 15$ GeV and $10 < E - P_Z < 45$ GeV. To further suppress non-$e\,p$ collisions we also require $\not{P}_t > 10$ GeV for calorimeter cells with $\theta > 10°$. The hadron system must exhibit large transverse energy ($E_t > 40$ GeV), and large invariant mass ($M > 55$ GeV). The polar angle of the final state neutrino, calculated from the hadron measurements assuming that the $\nu_e\, q\, \overline{q}$ system conserves the longitudinal momentum variable ($E - P_Z = 2E_e$) and transverse momentum ($\not{P}_t = 0$), is required to be less than 140°.

The acceptance for the $\nu_e\, q\, \overline{q}$ final state is approximately 65% for e^* production, and 75% for ν^* production. The total number of events observed in data is 13, compared with a background expectation of 8.4 ± 1.5 predominantly from charged current DIS, as seen in Tab. 1.

The mass of the neutrino-boson system, $M_{\nu V}$, is calculated from the measured quantities $\not{P}_t$ and $\delta \equiv E - P_Z$. With the assumptions described above, the invariant mass is

$$M^2_{\nu V} \;=\; \frac{4\, \not{P}_t^{\,2} E_e^2 + 2E_e M_V^2 (2E_e - \delta)}{\delta(2E_e - \delta)} \tag{11}$$

Here E_e is the electron beam energy and M_V is the mass of the gauge boson. The unshaded histogram in Fig. 4 shows the expected lineshape for an excited electron of mass 225 GeV. The mass resolution determined from Monte Carlo simulations is approximately 9 GeV (14 GeV) for excited electrons (excited neutrinos).

The invariant mass distribution for the selected events with the $e^* \to \nu_e W$ hypothesis is shown in Fig. 4 for data (solid points) compared with the Monte Carlo background (shaded histogram). No evidence for a peak is seen. The Kolmogorov test applied to the mass distribution yields a probability of 55% that the shape of the observed distribution arises from the expected background.

6.4 $\nu_e\, \gamma$ Resonance Search

This final state could occur if neutrinos contained charged constituents. The principal signature is an isolated electromagnetic cluster in events with missing transverse momentum. Backgrounds arise from charged current DIS events with isolated π^0s or initial state radiation.

A photon is tagged by identifying an EM cluster with more than 15 GeV of transverse energy. The cluster is required to be isolated in an η–ϕ cone of radius $R = 0.7$ (see

Section 5). A photon candidate is rejected if a track measured by the central tracking detector with $\theta > 15^\circ$ projects to within 40 cm of the cluster.

The presence of a neutrino is inferred by requiring $\not\!\!P_{\rm t}$> 15 GeV. The recoil jet typically associated with ν^* production is identified by requiring $E_{\rm t,had} > 10$ GeV. Neutral current DIS events are suppressed by requiring $E - P_{\rm Z} < 50$ GeV.

No event survives the selection criteria. The background expected from charged current DIS is 0.4 ± 0.1 events. The acceptance for the $\nu_{\rm e}\,\gamma$ final state is approximately 50%.

6.5 $e\,\nu\,\overline{\nu}$ Resonance Search

This final state could arise from production of an e^*, with subsequent decays: $e^* \to e\,Z^0$ and $Z^0 \to \nu\overline{\nu}$; or $e^* \to \nu_{\rm e}\,W$ and $W \to e\,\nu_{\rm e}$.[6] Such events would contain a striking signature: one high $E_{\rm t}$ electron in the detector, and nothing else except for a possible low $E_{\rm t}$ recoil jet. Backgrounds from charged and neutral current DIS are small. A rare Standard Model background process is W production.

The electron is tagged by identifying an EM cluster with more than 15 GeV of transverse energy. The cluster must be isolated in an η–ϕ cone of radius $R = 0.7$ and be accompanied by a track with momentum larger than 10 GeV that projects to within 40 cm of the cluster.

Events are expected to have missing transverse and longitudinal momentum, so $\not\!\!P_{\rm t}$> 15 GeV and $E - P_{\rm Z} < 45$ GeV are required. If a recoil jet is present, it is not expected to be back-to-back in azimuth with the electron because of the transverse momentum carried by the final state neutrinos. Consequently, if the hadronic transverse energy $E_{\rm t,had}$ is larger than 2 GeV, we require $\cos(\phi_{\rm e} - \phi_{\rm had}) > -0.95$. The acceptance for this final state is approximately 70% for $e^* \to e\,Z^0$ decays, and 60% for $e^* \to \nu_{\rm e}\,W$ decays.

One event survives the selection criteria, with mass $M_{eZ} = 116$ GeV. The expected background, itemized in Tab. 1, is 1.0 ± 0.2 events.

6.6 $e\,\overline{e}\,\nu_{\rm e}$ Resonance Search

The selection for $\nu_{\rm e}^* \to e\,W \to e\,\overline{e}\,\nu_{\rm e}$ is a variation of the $e\,\nu\,\overline{\nu}$ selection criteria discussed in the previous section. These decays would feature two high transverse energy EM clusters, missing transverse momentum, and a possible recoil jet from the struck proton.

We require two EM clusters, each with more than 10 GeV of transverse energy. No isolation cut is applied, and no explicit track match is made. The presence of a neutrino is inferred by requiring $\not\!\!P_{\rm t}$> 15 GeV. Since the two electrons can carry a substantial amount of the $\nu_{\rm e}^*$ momentum, only the loose cut $E - P_{\rm Z} < 65$ GeV is applied.

The acceptance for the $e\,\overline{e}\,\nu_{\rm e}$ final state is approximately 60%. No event survives the cuts. The expected background is very small, and is assumed negligible for the purposes of setting cross section upper limits.

[6] Other decays which lead to missing transverse momentum in the calorimeter (e.g., $Z^0 \to \mu^+\mu^-, \tau^+\tau^-$, etc.) would also be selected with lower efficiency; these decays are not used in calculating the sensitivity.

6.7 $q\,\gamma$ Resonance Search

Events with excited quarks (q^*) share some characteristics with low Q^2 DIS events and with photoproduction processes, in that the scattered electron might enter the detector or travel in the direction of the electron beam and miss the detector. Hence, one cannot cut tightly on $E - P_Z$, and the cut on $E_{\rm rear}$ must be relaxed from that used for the excited lepton searches. We require either $E_{\rm rear} < 2$ GeV, or else $E_{\rm rear} < 10$ GeV and the electromagnetic fraction of the calorimeter energy in the rear direction is larger than 90%. This removes most low Q^2 neutral current DIS events and resolved photoproduction events, while retaining efficiency for excited quarks which typically have only a low energy electron in the rear direction.

A resonance in the photon-jet invariant mass spectrum would provide compelling evidence for the decay $q^* \to q\,\gamma$. Photons are selected by identifying an EM cluster with more than 15 GeV of transverse energy. The cluster is required to be isolated in a large η–ϕ cone of radius $R = 1.5$, a larger cone than used in the other searches to reduce the large rate from π^0s produced in the jets of photoproduction reactions. A photon candidate is rejected if a track measured by the central tracking detector with $\theta > 15°$ projects to within 40 cm of the EM cluster.

The photon and hadron (see Sec. 5) polar angles must be in the forward region: $\theta_\gamma < 80°$and $\theta_{\rm had} < 100°$. The total transverse energy measured for the event must be large: $E_{\rm t}> 30$ GeV.

The measured longitudinal momentum variable will not in general satisfy the relation, $E - P_Z = 2E_e$, for events containing excited quarks. However, the heavy q^* is produced with little transverse momentum, which permits the $q\gamma$ invariant mass, $M_{q\gamma}$, to be calculated optimally from E_γ, θ_γ, and $\theta_{\rm had}$:

$$M^2_{q\gamma} \;=\; 2\,E^2_\gamma\,\frac{\sin\theta_\gamma}{\sin\theta_{\rm had}}\left[1-\cos(\theta_\gamma+\theta_{\rm had})\right] \qquad (12)$$

The mass resolution determined from Monte Carlo simulations varies from 3 GeV at a mass of 40 GeV to 8 GeV at a mass of 150 GeV. The unshaded histogram in Fig. 5 shows the expected lineshape for an excited quark of mass 150 GeV.

The overall acceptance for events with $q^* \to q\,\gamma$ varies from 20% at a mass of 40 GeV to 65% for masses above 150 GeV. The total number of events selected from data is 18, compared with a total background expectation of 23.5 ± 2.5 events, tabulated in detail in Tab. 1.

The $q\,\gamma$ invariant mass distribution for the selected events is presented in Fig. 5 for data (solid points) compared with the Monte Carlo background (shaded histogram). The spectrum shows no evidence for a resonance. The Kolmogorov test applied to the mass spectrum yields a probability of 47% that the observed distribution conforms to the expected background shape.

6.8 $q\,\overline{e}\,\nu_e$ Resonance Search

We address here the case of excited quarks decaying through the chain: $q^* \to q\,W$, with $W \to \overline{e}\,\nu_e$. The final state contains a neutrino, an electron, and a jet which is not back-to-back in azimuth with the electron. Each has high transverse momentum, so backgrounds from DIS and photoproduction are expected to be minimal. The selection criteria for the $q\,\overline{e}\,\nu_e$ search are similar to those used for the $e\,\nu\,\overline{\nu}$ search, except that the hadron system from the decay quark must be identified and the cut on $E_{\rm rear}$ is as discussed in the previous section.

The electron is tagged by identifying an EM cluster with more than 15 GeV of transverse energy. The cluster is required to be isolated in an η–ϕ cone of radius $R = 0.7$. No explicit track match is demanded. Since a high transverse momentum neutrino is expected, $\not\!\!P_t >$ 15 GeV is imposed. The upper bound on $E - P_Z$ is relaxed to 65 GeV since the scattered electron may enter the detector. The energetic hadron system is identified by selecting events with $E_{t,\rm had} > 10$ GeV. Since the hadronic jet is not expected to be back-to-back in azimuth with the electron, the cut $\cos(\phi_e - \phi_{\rm had}) > -0.95$ is applied.

The acceptance for the $q\,\overline{e}\,\nu_e$ final state is approximately 50%. No event survives the selection criteria. The total background expected is 1.5 ± 0.3 events, roughly equally from neutral current and charged current DIS processes, as described in Tab. 1.

7 Systematic Uncertainties

The overall uncertainty on the normalizations for the backgrounds and signals in these searches receives contributions from the acceptance and luminosity, as well as theoretical uncertainties on the production mechanisms. Our evaluation of these are itemized below. Experimental errors are listed first.

- The uncertainty on the measured integrated luminosity of the combined 1994 and 1995 e^+p data sample is 1.5%.
- The uncertainty on the electron/photon identification efficiency is estimated to be at most 5%, determined by comparing alternate algorithms for EM cluster identification.
- The sensitivity of event selection to vertex reconstruction algorithms and the underlying vertex distribution is estimated to produce uncertainty at the 4% level.
- The systematic 3% uncertainty in the calorimeter energy scale is found to lead to an overall 3% uncertainty in the acceptance.
- Since calculations use smooth parameterizations of the excited fermion acceptances as functions of the f^* mass, some error is incurred by interpolation between generated Monte Carlo mass points. This uncertainty is estimated to be 4%.

- The effects of errors on background estimates used in the upper limit derivation depend on the number of observed events as well as the size of the background. However, 10% variations of the background normalization typically lead to variations of 6% or less on upper limits.

- The theoretical uncertainty introduced by radiative corrections to the excited fermion production model and the uncertainty associated with the parton density distributions used to model the proton is taken to be 8%, as determined from our earlier study [1].

- The model dependence of the excited fermion angular decay distribution is evaluated by comparing the acceptance for isotropic decays versus the nominal [3, 7] distribution.[7] The deviation is typically 5% or less.

Adding all contributions in quadrature yields a total systematic uncertainty of 14%, which is incorporated into the upper limit procedure described in the Appendix.

8 Results

We have no positive evidence for excited leptons or quarks in any of the 8 searches (11 excited fermion decay chains) described above. The data provide upper limits (U.L.) as a function of the excited fermion mass, M_{f^*}, on the production cross section times branching ratio:

$$(\sigma \cdot BR)_{\text{U.L.}} = \frac{N_{\text{U.L.}}(M_{f^*})}{A(M_{f^*}) \cdot L} \tag{13}$$

where L is the integrated luminosity and $A(M_{f^*})$ is the parameterized acceptance for the excited fermion decay including, when appropriate, the branching fraction of the Z^0 or W decay. The upper limit on the number of signal events, $N_{\text{U.L.}}$, is calculated at the 95% confidence level as a function of mass according to an unbinned likelihood technique. This procedure, including its use to obtain combined upper limits for cases with more than one decay chain, is described in the Appendix.

The resulting upper limit curves on the production cross sections are shown in Fig. 6 for excited electrons, Fig. 7 for excited neutrinos, and Fig. 8 for excited quarks. For final states with photons, the limits are typically less than 1 pb, an order of magnitude improvement over our previous upper limits [1]. The limits are below those reported by H1 [2] because this ZEUS sample uses a larger integrated luminosity.

We also set upper limits on coupling strengths in the compositeness model described by the Lagrangian (2), with the relationship fixed among the $SU(2)_L$, $U(1)_Y$, and $SU(3)_C$ coupling constants: f, f', and f_s, respectively. Branching fractions are then determined and cross sections calculated in terms of a single unknown parameter, f/Λ. The upper

[7] For $f^* \to f\gamma$, for example, the nominal decay distribution is $(1 + \cos\theta^*)$, where θ^* is the polar angle between the incoming and outgoing fermion in the f^* rest frame.

limit at the 95% confidence level is obtained from the upper limit $(\sigma \cdot BR)_{\rm U.L.}$ by using the relation

$$\left(\frac{f}{\Lambda}\right)_{\rm U.L.} = \sqrt{\frac{(\sigma \cdot BR)_{\rm U.L.}}{\sigma_{\rm MC} \cdot BR}} \left(\frac{f}{\Lambda}\right)_{\rm MC} \tag{14}$$

where BR is the branching ratio, and $\sigma_{\rm MC}$ is the Monte Carlo prediction for the theoretical cross section calculated using the coupling $(f/\Lambda)_{\rm MC}$.

For excited leptons, the parameter $f_{\rm s}$ is irrelevant. For e^*, we choose $f = f'$. For $\nu_{\rm e}^*$, we set $f = -f'$ (see Section 2).

For excited quarks, we choose $f = f'$ and $f_{\rm s} = 0$. Given the stringent limits[10, 11] on $f_{\rm s}$ set by CDF on q^* production, we have chosen to concentrate on the unique HERA sensitivity at high mass to electroweak couplings: f and f'. We further assume transitions to a single excited mass degenerate doublet (u^*, d^*) such that the production cross section is the sum of both u and d quark excitations.[8]

The upper limits on f/Λ as a function of mass are shown in Fig. 9 for e^*, in Fig. 10 for $\nu_{\rm e}^*$, and in Fig. 11 for q^*. These limits are derived under the narrow width approximation. For higher masses and couplings than reported here, the natural width becomes much larger than the experimental width. The e^* and q^* searches encompass multiple decay modes; the combined limits are shown as dashed lines in each figure. Figure 10 shows the limit on $\nu_{\rm e}^*$ from the previous search by ZEUS [1] in e^-p collisions with a much lower luminosity (0.55 pb^{-1}). This previous limit is superior to that presented here for $M_{\nu^*} > 130$ GeV because the e^-p cross section is significantly higher at large $\nu_{\rm e}^*$ masses.[9]

The coupling limit from the excited electron search corresponds to a lower limit on the compositeness scale $\Lambda/f \approx 1$ TeV for $30 < M_{e^*} < 100$ GeV. Similar sensitivity is evident from the excited quark search, for q^* with dominantly electroweak couplings ($f_s = 0$).

It is possible to set mass limits on excited fermions from the limit curves on f/Λ versus M_{f^*} if one makes the further assumption that $f/\Lambda = 1/M_{f^*}$.[10] For this case, excited electrons are ruled out at the 95% confidence level in the mass interval 30–200 GeV using the combined limit from all three decay modes. Excited neutrinos are excluded over the range 40–96 GeV. Excited quarks with only electroweak coupling are excluded over the range 40–169 GeV using the combined limit from $q^* \to q\,\gamma$ and $q^* \to q\,W$.

The LEP experiments have recently reported searches [8, 9] for excited leptons operating with center-of-mass energies $\sqrt{s} = 161$ GeV and $\sqrt{s} = 130$–140 GeV (LEP upper limits

[8] The branching ratio used in the calculation is a weighted average; the weights are based on the square of the quark charges and the x-dependent relative density of u and d quarks in the proton. Because q^* are produced via photon exchange at HERA, our limits are primarily sensitive to u quark excitations.

[9] The cross section for massive ν^* production in e^+p scattering is heavily suppressed relative to e^-p scattering, partly because of the smaller density of valence d quarks to valence u quarks (large Bjorken x is required), but mainly because the chiral nature of the W exchange results in suppressed particle-antiparticle coupling amplitudes at large energy transfers. For $M_{\nu^*} > 130$ GeV, the cross section advantage for e^- beam exceeds the luminosity advantage for e^+ beam. High luminosity with e^- beam will substantially improve these limits.

[10] In the Lagrangian convention of the Particle Data Group [31] for excited fermion transitions, our mass limits correspond to $\lambda_\gamma > 1$ for excited electrons, $\lambda_W > 1/\sqrt{2}$ for excited neutrinos, and $\lambda_\gamma > \frac{2}{3}$ for excited u quarks.

on λ/M_{l^*} must be multiplied by $\sqrt{2}$ to be compared with our limits on f/Λ). The LEP single and pair production upper limits on excited electrons ($f = f'$) and excited electron neutrinos ($f = -f'$) are shown by the shaded lines in Figs. 9 and 10. The region above and to the left of the lines is excluded at the 95% confidence level. The sensitivity to excited leptons above the pair production threshold and below 160–170 GeV is slightly better than reported here, but the present analysis extends these limits to well beyond 170 GeV for excited electrons.

9 Summary

We have searched for heavy excited states of electrons, neutrinos, and quarks using 9.4 pb^{-1} of e^+p collisions at a center-of-mass energy of 300 GeV recorded with the ZEUS detector at HERA. No evidence of a signal was found in any of eight distinct decay topologies. Upper limits at the 95% confidence level are derived on the production cross section times branching ratio which are typically an order of magnitude better than our previous limits from e^-p collisions. We also set upper limits on the coupling f/Λ as a function of the excited fermion mass. With the choice $f/\Lambda = 1/M_{f^*}$, we exclude excited electrons with mass between 30 and 200 GeV, excited electron neutrinos with mass between 40 and 96 GeV, and excited quarks coupled electroweakly with mass between 40 and 169 GeV.

Acknowledgements

We appreciate the contributions to the construction and maintenance of the ZEUS detector by many people who are not listed as authors. We especially thank the DESY computing staff for providing the data analysis environment and the HERA machine group for their outstanding operation of the collider. Finally, we thank the DESY directorate for strong support and encouragement.

Appendix

The procedure used for calculating the upper limit curves on excited fermion (of mass, M_f^*) production is obtained from the spectrum in observed mass, M. The formulation can be derived starting with the Poisson likelihood for observing n events:

$$\mathcal{L}(\mu_s;\, n, \mu_b) \;=\; \frac{1}{n!}\, e^{-(\mu_s+\mu_b)}\, (\mu_s + \mu_b)^n \tag{15}$$

Here μ_s is the average number of expected signal events and μ_b is the average number of expected background events. The upper limit on μ_s at the 95% confidence level, $N_{\mathrm{U.L.}}$, is obtained by solving the integral equation:

$$\int_0^{N_{\mathrm{U.L.}}} \mathcal{L}(\mu_s;\, n, \mu_b)\, d\mu_s \;=\; 0.95 \int_0^{\infty} \mathcal{L}(\mu_s;\, n, \mu_b)\, d\mu_s \tag{16}$$

The solution to Eq. (16) using the likelihood of Eq. (15) reduces to the convention recommended by the Particle Data Group [32] for setting upper limits in the presence of background.

For the application relevant to this work, we divide the total number of observed events, n, into a spectrum in observed mass, M. The bin size, dM, is chosen small enough so that there is at most one event in any single bin. The likelihood function corresponding to a signal with mass M_{f^*} is then the product of the likelihoods from each bin. This likelihood reduces to

$$\mathcal{L}(M_{f^*}) \;=\; \exp[-(\mu_s(M_{f^*}) + \mu_b)] \prod_{j \in \text{events}}^{n} (\mu_{s,j}(M_{f^*}) + \mu_{b,j}) \tag{17}$$

where $\mu_s(M_{f^*})$ and μ_b are the total number of expected signal and background events, respectively. The signal and background populations in each bin are given by

$$\mu_{s,j}(M_{f^*}) \;=\; G(M_{f^*}, M)\Big|_{M=M_j} dM \tag{18}$$

$$\mu_{b,j} \;=\; B(M)\Big|_{M=M_j} dM \tag{19}$$

where M_j is the mass corresponding to observed event j. The differential background contribution $B(M)$ is obtained from a fit to the Monte Carlo calculated spectrum. The signal contribution expected from the experiment is assumed to have a Gaussian lineshape, $G(M_{f^*}, M)$, with peak values and widths parameterized as a function of M_{f^*}. These are obtained from Gaussian fits to Monte Carlo generated mass spectra.[11]

Inserting these parameterizations into Eq. (17) provides a likelihood (up to multiplication by bin size) at each value of excited fermion mass, M_{f^*}. Substituting into Eq. (16), we observe that the bin size, dM, cancels on both sides of the equation. The solution to this integral equation provides at each M_{f^*} the value for $N_{\text{U.L.}}$, the 95% confidence limit on the number of events.

It is straightforward to generalize this upper limit determination for the case when two decay modes of the same excited fermion are considered. The overall likelihood is the product of the individual likelihoods for each separate decay chain:

$$\begin{aligned}\mathcal{L}(M_{f^*}) \;=\; \mathcal{L}_1(M_{f^*})\,\mathcal{L}_2(M_{f^*}) \;=\; \exp[-(\mu_s(M_{f^*}) + \mu_b^{(1)} + \mu_b^{(2)})] \\ \times \prod_{i \in \text{events}}^{n_1} \left[\Big(\frac{A_1}{A_1 + A_2}\Big) \mu_{s,i}(M_{f^*}) + \mu_{b,i}^{(1)} \right] \prod_{j \in \text{events}}^{n_2} \left[\Big(\frac{A_2}{A_1 + A_2}\Big) \mu_{s,j}(M_{f^*}) + \mu_{b,j}^{(2)} \right]\end{aligned} \tag{20}$$

where $\mu_s(M_{f^*}) = \mu_s^{(1)} + \mu_s^{(2)}$ and A_i is the acceptance of the ith decay mode. The procedure for more than two decay chains is a trivial extension of this equation.

A systematic error from uncertainties in the acceptance and luminosity is included into the upper limit calculation by convoluting a Gaussian with the Poisson likelihood:

$$\mathcal{L}(\mu_s(M_{f^*});\, n, \mu_b) \to \int_0^\infty \frac{d\gamma}{\sqrt{2\pi}\delta} \exp[-(\gamma - 1)^2/2\delta^2]\; \mathcal{L}(\gamma\mu_s(M_{f^*});\, n, \gamma\mu_b) \tag{21}$$

[11] These spectra include experimental systematic and resolution effects only. The intrinsic lineshape of the excited fermion is assumed small (narrow width approximation).

where δ, the fractional systematic uncertainty, is taken to be 14% for the searches reported here. For the specific case when zero events are observed, this convolution increases $N_{\mathrm{U.L.}}$ from 3.0 to 3.2.

References

[1] ZEUS Collab., M. Derrick et al., Phys. Lett. **B316** (1993) 207;
ZEUS Collab., M. Derrick et al., Z. Phys. **C65** (1995) 627.

[2] H1 Collab., S. Aid et al., Nucl. Phys. **B483** (1997) 44.

[3] K. Hagiwara, S. Komamiya, and D. Zeppenfeld, Z. Phys. **C29** (1985) 115.

[4] J. Kühn and P. Zerwas, Phys. Lett. **B147** (1984) 189.

[5] F.M. Renard, Phys. Lett. **B116** (1982) 264;
F. del Águila, A. Méndez, and R. Pascual, Phys. Lett. **B140** (1984) 431;
M. Suzuki, Phys. Lett. **B143** (1984) 237.

[6] U. Baur, M. Spira, and P.M. Zerwas, Phys. Rev. **D42** (1990) 815.

[7] F. Boudjema, A. Djouadi, and J.L. Kneur, Z. Phys. **C57** (1993) 425.

[8] L3 Collab., M. Acciarri et al., Phys. Lett. **B370** (1996) 211;
DELPHI Collab., P. Abreu et al., Phys. Lett. **B380** (1996) 480;
ALEPH Collab., D. Buskulic et al., Phys. Lett. **B385** (1996) 445;
OPAL Collab., G. Alexander et al., Phys. Lett. **B386** (1996) 463.

[9] OPAL Collab., K. Ackerstaff et al., Phys. Lett. **B391** (1997) 197;
DELPHI Collab., P. Abreu et al., Phys. Lett. **B393** (1997) 245;
L3 Collab., M. Acciarri et al., Phys. Lett. **B401** (1997) 139.

[10] CDF Collab., F. Abe et al., Phys. Rev. Lett. **72** (1994) 3004.

[11] CDF Collab., F. Abe et al., Phys. Rev. Lett. **74** (1995) 3538;
CDF Collab., F. Abe et al., Phys. Rev. **D55** (1997) 5263.

[12] ZEUS Collab., M. Derrick et al., Phys. Lett. **B293** (1992) 465;

[13] The ZEUS Detector, Status Report 1993, DESY 1993.

[14] M. Derrick et al., Nucl. Inst. Meth. **A309** (1991) 77;
A. Andresen et al., Nucl. Inst. Meth. **A309** (1991) 101;
A. Bernstein et al., Nucl. Inst. Meth. **A336** (1993) 23.

[15] C. Alvisi et al., Nucl. Inst. Meth. **A305** (1991) 30.

[16] N. Harnew et al., Nucl. Inst. Meth. **A279** (1989) 290;
B. Foster et al., Nucl. Phys. B (Proc. Suppl.) **32** (1993) 181;
B. Foster et al., Nucl. Inst. Meth. **A338** (1994) 254.

[17] J. Andruszków et al., DESY 92–066 (1992).

[18] HEXF: H.J. Kim and S. Kartik, LSU Preprint LSUHE-145-1993.

[19] Ch. Berger and W. Wagner, Phys. Rep. **146** (1987) 1.

[20] LEPTO 6.1: G. Ingelman, in Physics at HERA, ed. W. Buchmuller and G. Ingelman (DESY, Hamburg 1991), vol. 3, 1366.

[21] JETSET 7.3: T. Sjöstrand and M. Bengtsson, Comp. Phys. Comm. **43** (1987) 367.

[22] A.D. Martin, W.J. Stirling, and R.G. Roberts, Phys. Rev. **D50** (1994) 6734.

[23] HERACLES 4.4: A. Kwiatkowski, H. Spiesberger, H.-J. Möhring, in Physics at HERA, ed. W. Buchmuller and G. Ingelman (DESY, Hamburg 1991), vol. 3, 1294.
A. Kwiatkowski, H. Spiesberger, and H.-J. Möhring, Z. Phys. **C50** (1991) 165.

[24] DJANGO 6.1: G.A. Schuler and H. Spiesberger, in Physics at HERA, ed. W. Buchmuller and G. Ingelman (DESY, Hamburg 1991), vol. 3, 1419.

[25] HERWIG 5.8: G. Marchesini et al., Comp. Phys. Comm. **67** (1992) 465.

[26] COMPTON 2.0: T. Carli et al., in Physics at HERA, ed. W. Buchmuller and G. Ingelman (DESY, Hamburg 1991), vol. 3, 1468.

[27] EPVEC: U. Baur, J.A.M. Vermaseren, and D. Zeppenfeld, Nucl. Phys. **B375** (1992) 3.

[28] GEANT 3.13: R. Brun et al., CERN DD/EE/84-1 (1987).

[29] H. Abramowicz, A. Caldwell, and R. Sinkus, Nucl. Inst. Meth. **A365** (1995) 508.

[30] W.T. Eadie, D. Drijard, F.E. James, M. Roos, and B. Sadoulet, Statistical Methods in Experimental Physics, (North Holland, Amsterdam and London, 1971) 269.

[31] Particle Data Group, R.M. Barnett et al., Phys. Rev. **D54** (1996) 1 (see p. 699).

[32] Particle Data Group, R.M. Barnett et al., *ibid*, (see p. 166).

Channel	Signature	A	$N_{\rm obs}$	$N_{\rm exp}$
$e^* \to e\,\gamma$	2 EM clusters	75%	103	97.5 ± 4.8 (COMPTON: 81.5) (NC DIS: 16.0)
$e^* \to e\,Z^0 \to e\,q\,\bar{q}$ $\nu_{\rm e}^* \to e\,W \to e\,q\,\bar{q}$	EM cluster large $E_{\rm t,had}$ and $M_{\rm had}$	55% 70%	21	15.3 ± 1.5 (NC DIS)
$e^* \to \nu_{\rm e}\,W \to \nu_{\rm e}\,q\,\bar{q}$ $\nu_{\rm e}^* \to \nu_{\rm e}\,Z^0 \to \nu_{\rm e}\,q\,\bar{q}$	$\not{P}_{\rm t}$ large $E_{\rm t,had}$ and $M_{\rm had}$	65% 75%	13	8.4 ± 1.5 (CC DIS: 4.8) (NC DIS: 1.0) (PHP: 2.6)
$\nu_{\rm e}^* \to \nu_{\rm e}\,\gamma$	$\not{P}_{\rm t}$ EM cluster (no track)	50%	0	0.4 ± 0.1 (CC DIS)
$e^* \to e\,Z^0 \to e\,\nu\,\bar{\nu}$ $e^* \to \nu_{\rm e}\,W \to e\,\nu_{\rm e}\,\bar{\nu}_{\rm e}$	$\not{P}_{\rm t}$ EM cluster (track)	70% 60%	1	1.0 ± 0.2 (CC DIS: 0.1) (NC DIS: 0.45) (W PROD'N: 0.45)
$\nu_{\rm e}^* \to e\,W \to e\,\overline{e}\,\nu_{\rm e}$	$\not{P}_{\rm t}$ 2 EM clusters	60%	0	≈ 0
$q^* \to q\,\gamma$	EM cluster (no track) large $E_{\rm t,had}$	60%	18	23.5 ± 2.5 (PROMPT γ: 14.4) (PHP: 5.1) (NC DIS: 4.0)
$q^* \to q\,W \to q\,\overline{e}\,\nu_{\rm e}$	$\not{P}_{\rm t}$ EM cluster large $E_{\rm t,had}$	50%	0	1.5 ± 0.3 (CC DIS: 0.5) (NC DIS: 0.75) (W PROD'N: 0.2)

Table 1: The f^* decay signature, typical acceptance (A), number of observed events ($N_{\rm obs}$), and number of expected background events ($N_{\rm exp}$) for the excited fermion decay topologies investigated.

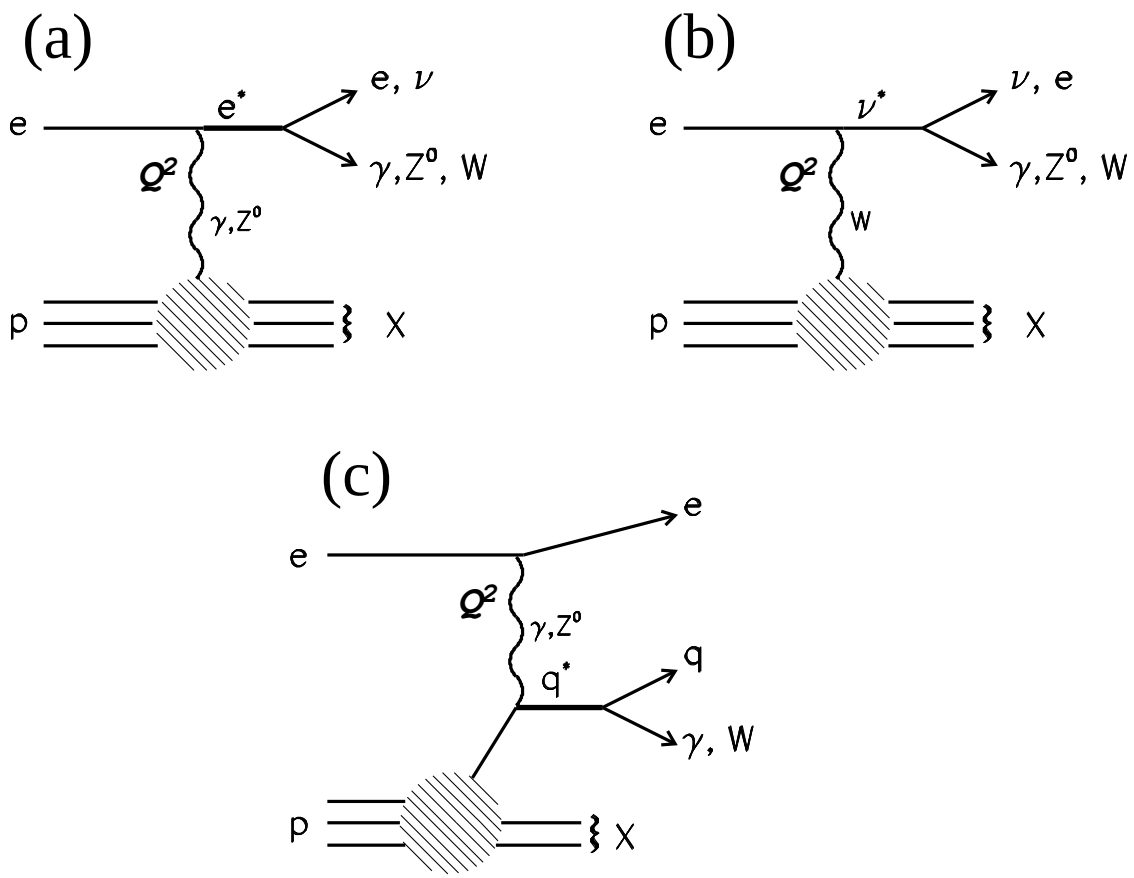

Figure 1: Diagrams for the production of (a) excited electrons, (b) excited neutrinos, and (c) excited quarks in $e\,p$ collisions. Only those decay modes considered in this paper are shown.

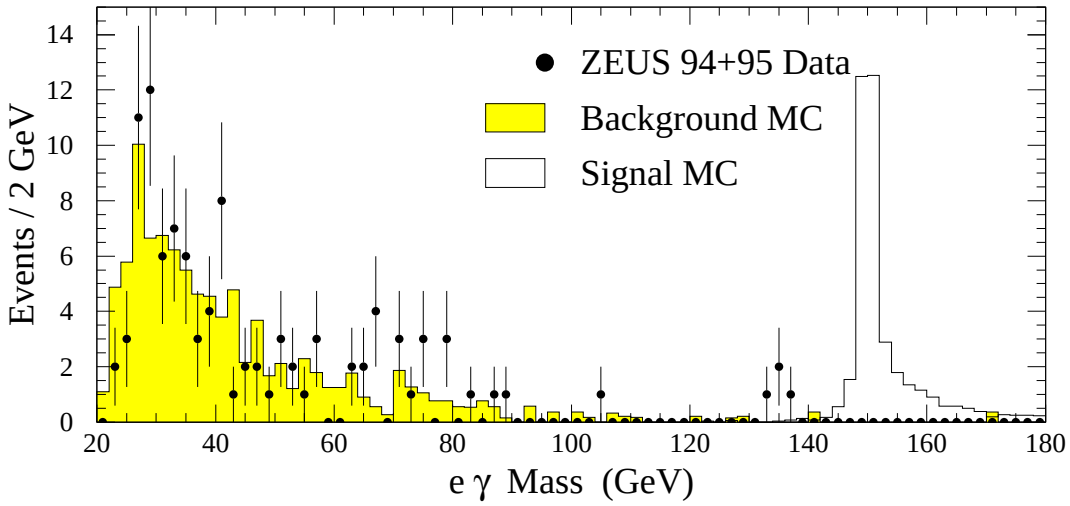

Figure 2: Distribution of the $e\,\gamma$ invariant mass for $e^* \to e\,\gamma$ candidates. Solid points show ZEUS data, and the shaded histogram represents the expected background. The unshaded histogram shows the expected lineshape for a 150 GeV excited electron (assuming $f = f'$ and $f/\Lambda = 8.0 \times 10^{-3}$ GeV^{-1}).

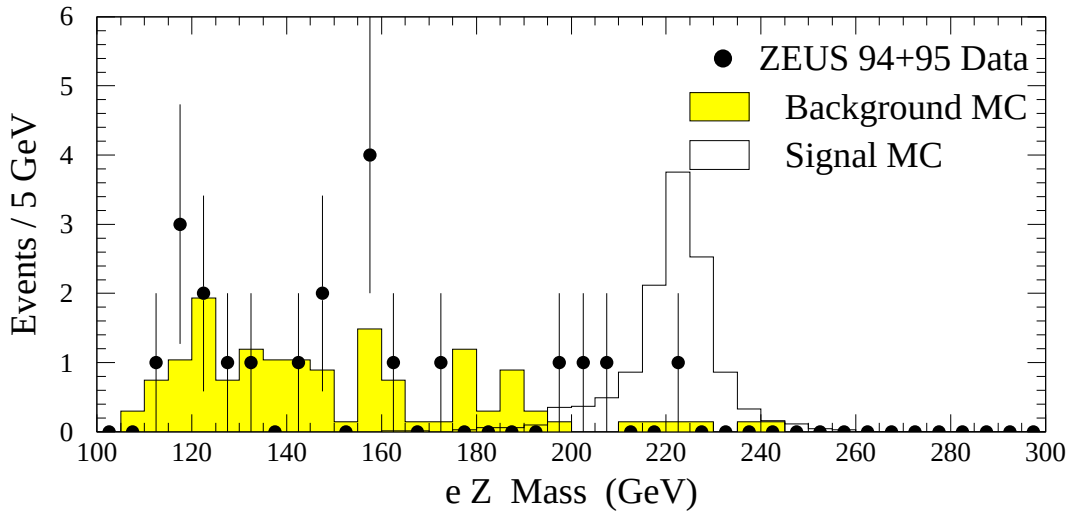

Figure 3: Distribution of the $e\,Z$ invariant mass for $e^* \to e\,Z^0 \to e\,q\,\overline{q}$ candidates. Solid points show ZEUS data, and the shaded histogram represents the expected background. The unshaded histogram shows the expected lineshape for a 225 GeV excited electron (assuming $f = f'$ and $f/\Lambda = 5.0 \times 10^{-2}$ GeV^{-1}).

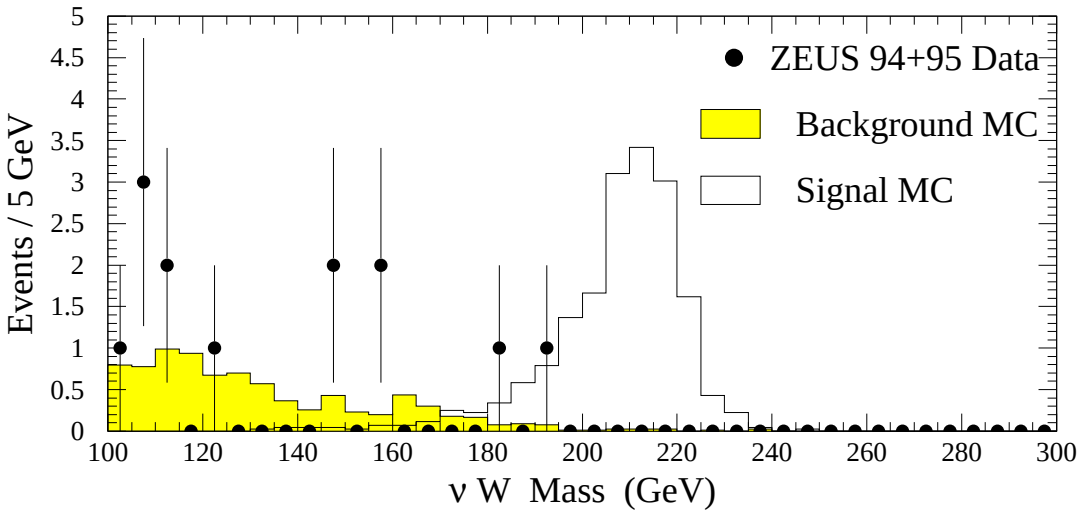

Figure 4: Distribution of the $\nu_e W$ invariant mass for $e^* \to \nu_e W \to \nu_e q\overline{q}$ candidates. Solid points show ZEUS data, and the shaded histogram represents the expected background. The unshaded histogram shows the expected lineshape for a 225 GeV excited electron (assuming $f = f'$ and $f/\Lambda = 2.5 \times 10^{-2}$ GeV^{-1}). The peak is shifted to lower mass because the measured hadronic energy is not explicitly corrected for losses.

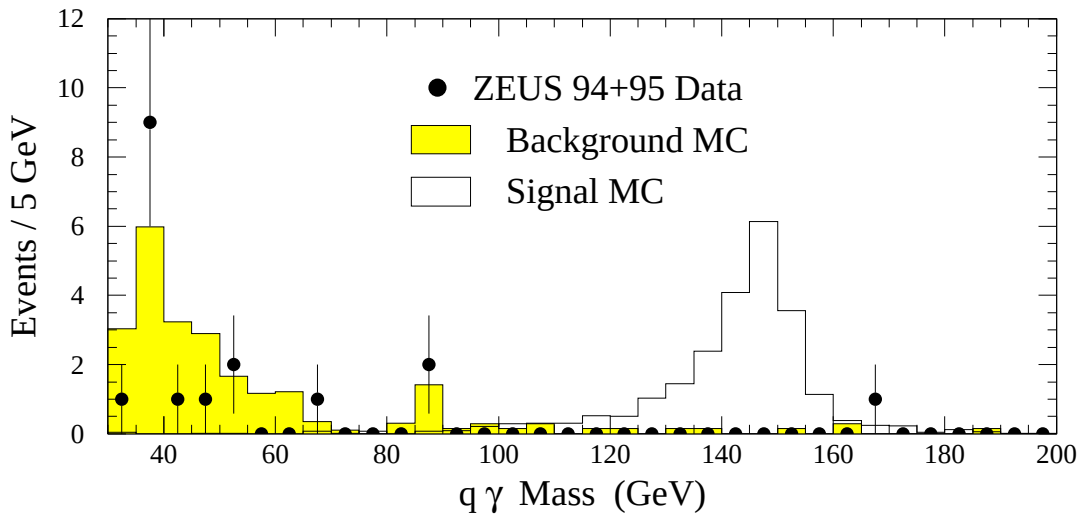

Figure 5: Distribution of the $q\gamma$ invariant mass for $q^* \to q\gamma$ candidates. Solid points show ZEUS data, and the shaded histogram represents the expected background. The unshaded histogram shows the expected lineshape for a 150 GeV excited quark (assuming $f_s = 0$, $f = f'$, and $f/\Lambda = 1.0 \times 10^{-2}$ GeV^{-1}).

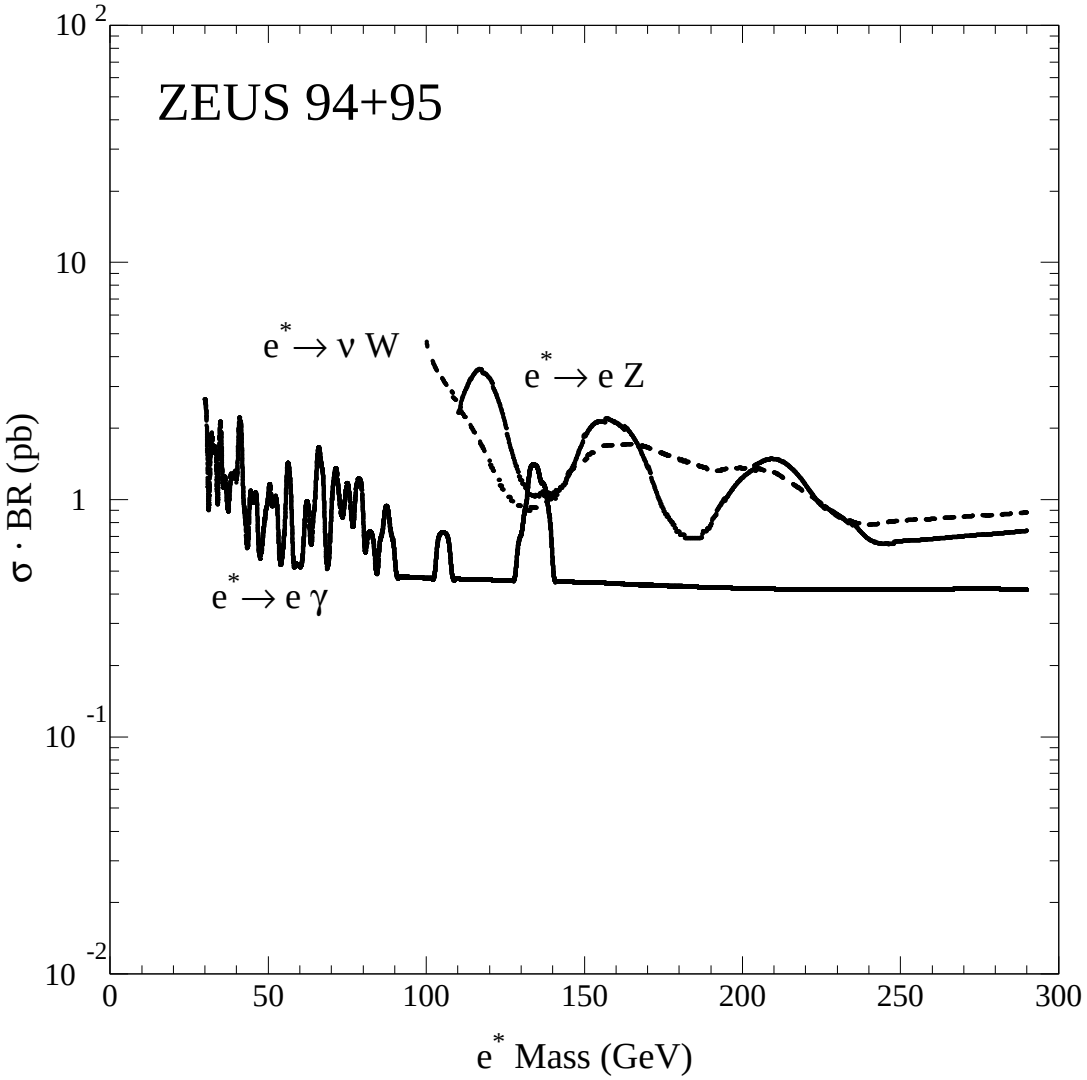

Figure 6: Upper limits at the 95% confidence level on the product of the production cross section (in picobarns) for the process $e^+ p \to e^* X$ and the branching ratio for $e^* \to \ell V$ as a function of mass for the studied e^* channels.

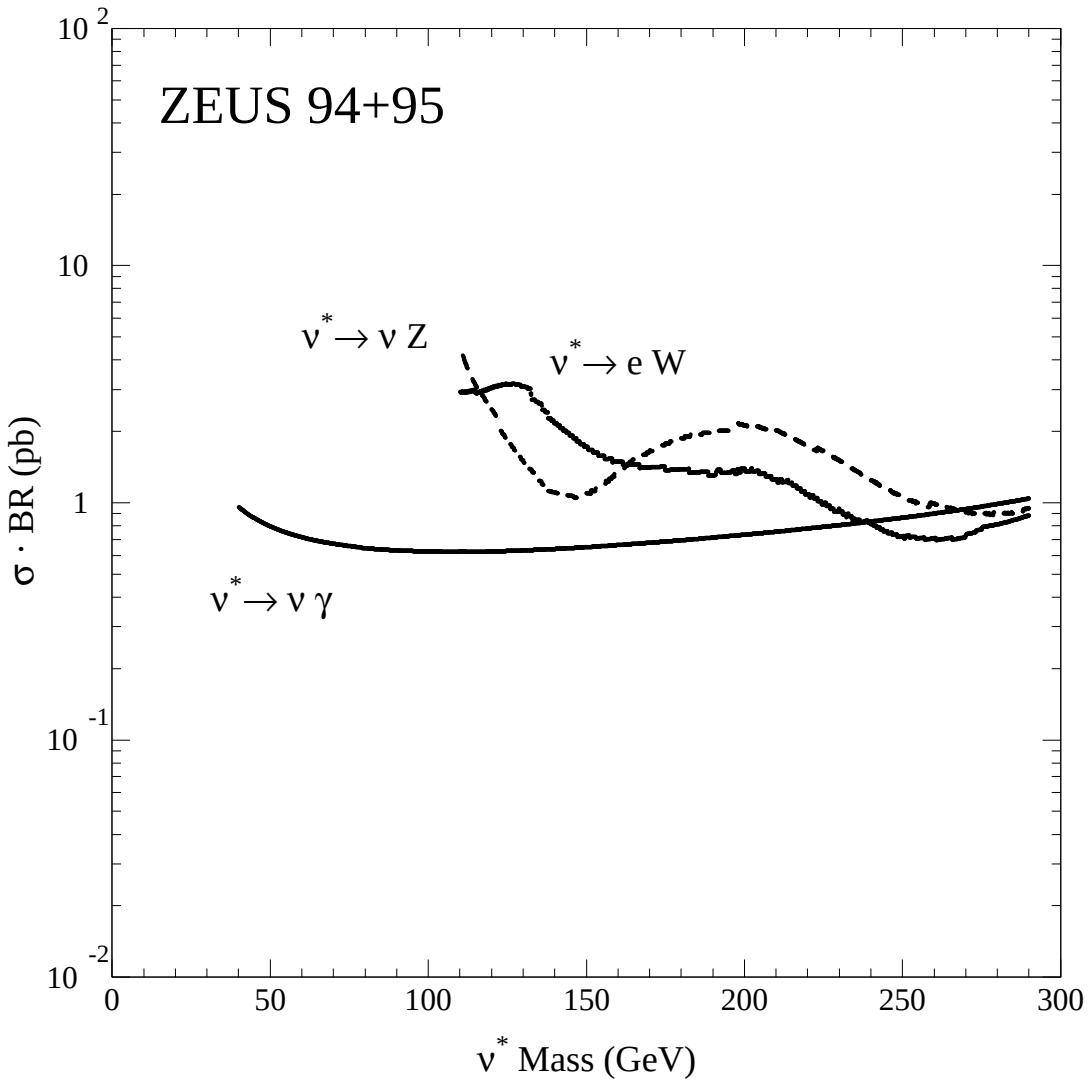

Figure 7: Upper limits at the 95% confidence level on the product of the production cross section (in picobarns) for the process $e^+ p \to \nu_e^* X$ and the branching ratio for $\nu_e^* \to \ell V$ as a function of mass for the studied ν_e^* channels.

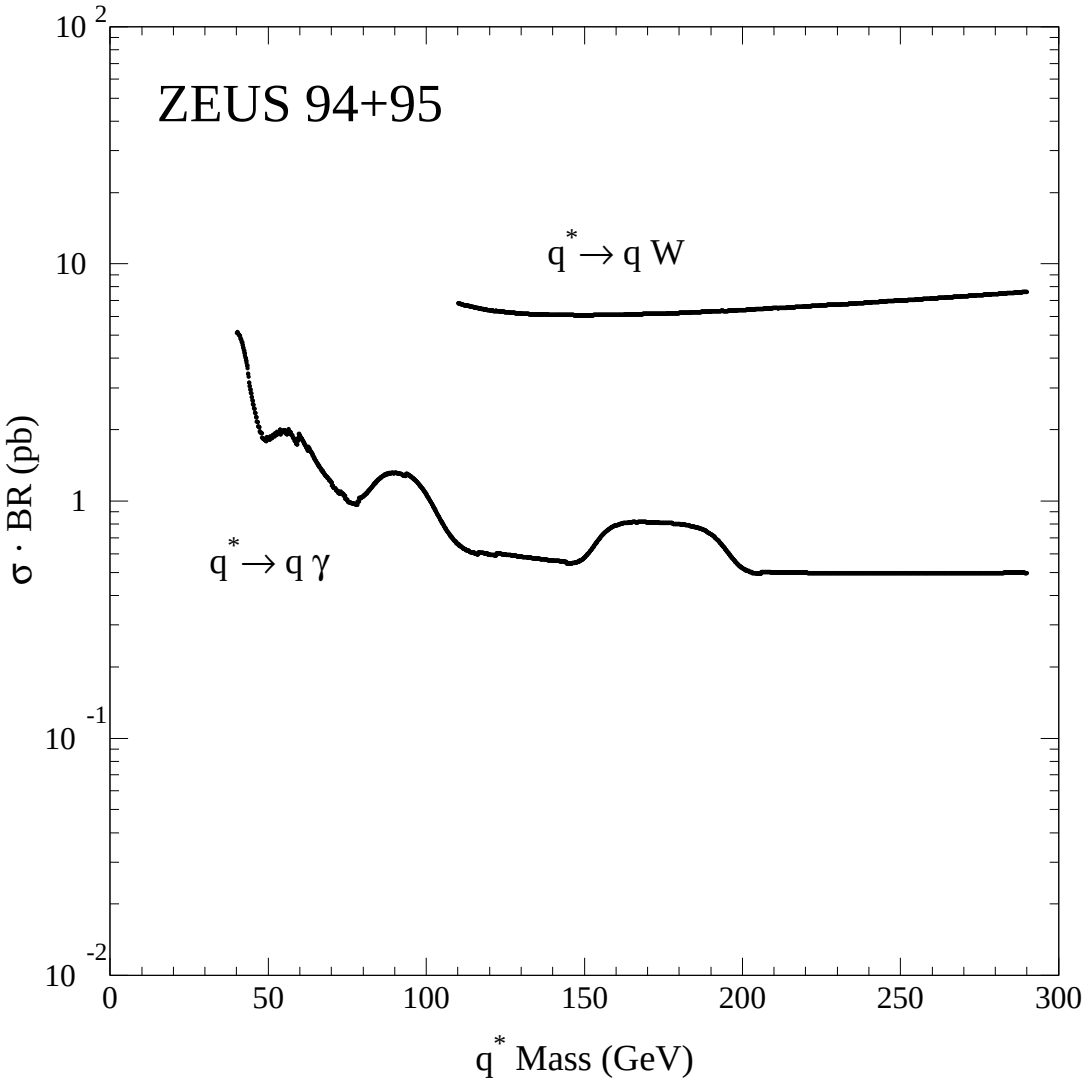

Figure 8: Upper limits at the 95% confidence level on the product of the production cross section (in picobarns) for the process $e^+ p \to e^+ q^* X$ and the branching ratio for $q^* \to q V$ as a function of mass for the studied q^* channels.

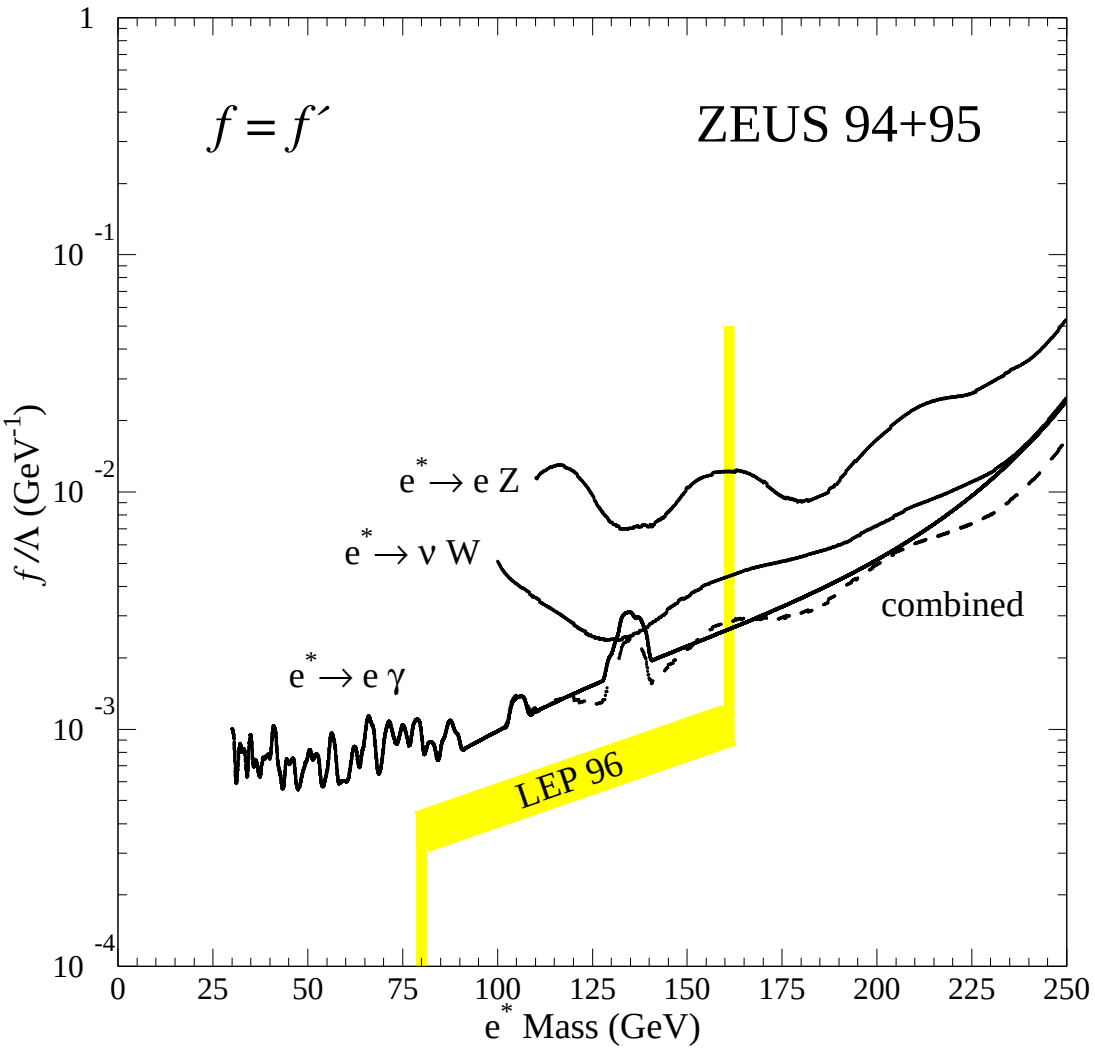

Figure 9: Upper limits at the 95% confidence level on the coupling f/Λ as a function of mass for the excited electron channels assuming $f = f'$. The dashed line is the combined limit from all three decay modes. The shaded line is the limit reported recently by the LEP experiments [8, 9], where the limit variations between 80 and 161 GeV are given approximately by the line width.

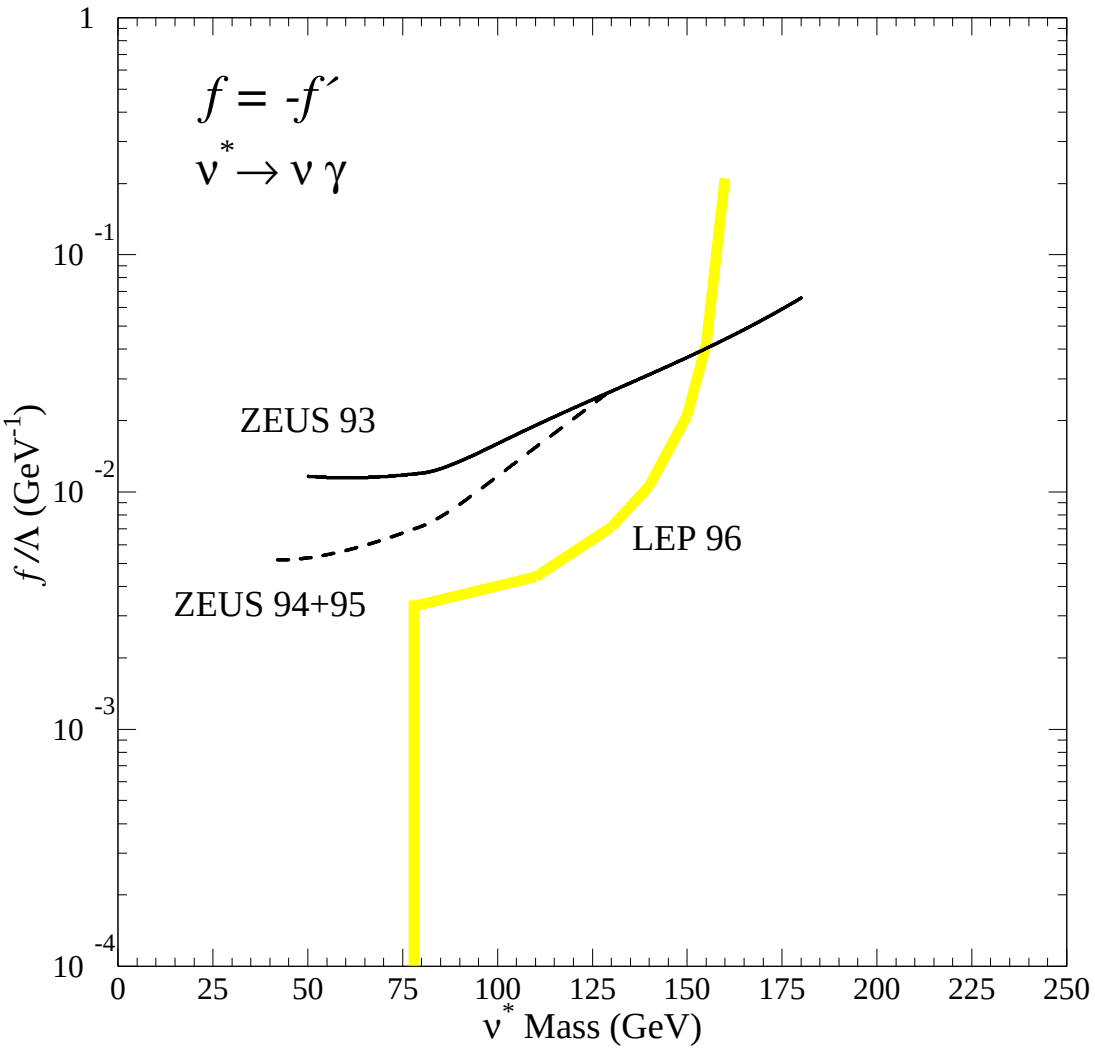

Figure 10: Upper limits at the 95% confidence level on the coupling f/Λ as a function of mass for the $\nu_e^* \to \nu_e \gamma$ channel only assuming $f = -f'$. The dashed line is the limit derived from this analysis, whereas the solid line is the corresponding limit from our previous analysis [1] of $e^- p$ collisions. The limit from the LEP experiments [8, 9] is shown by the shaded line.

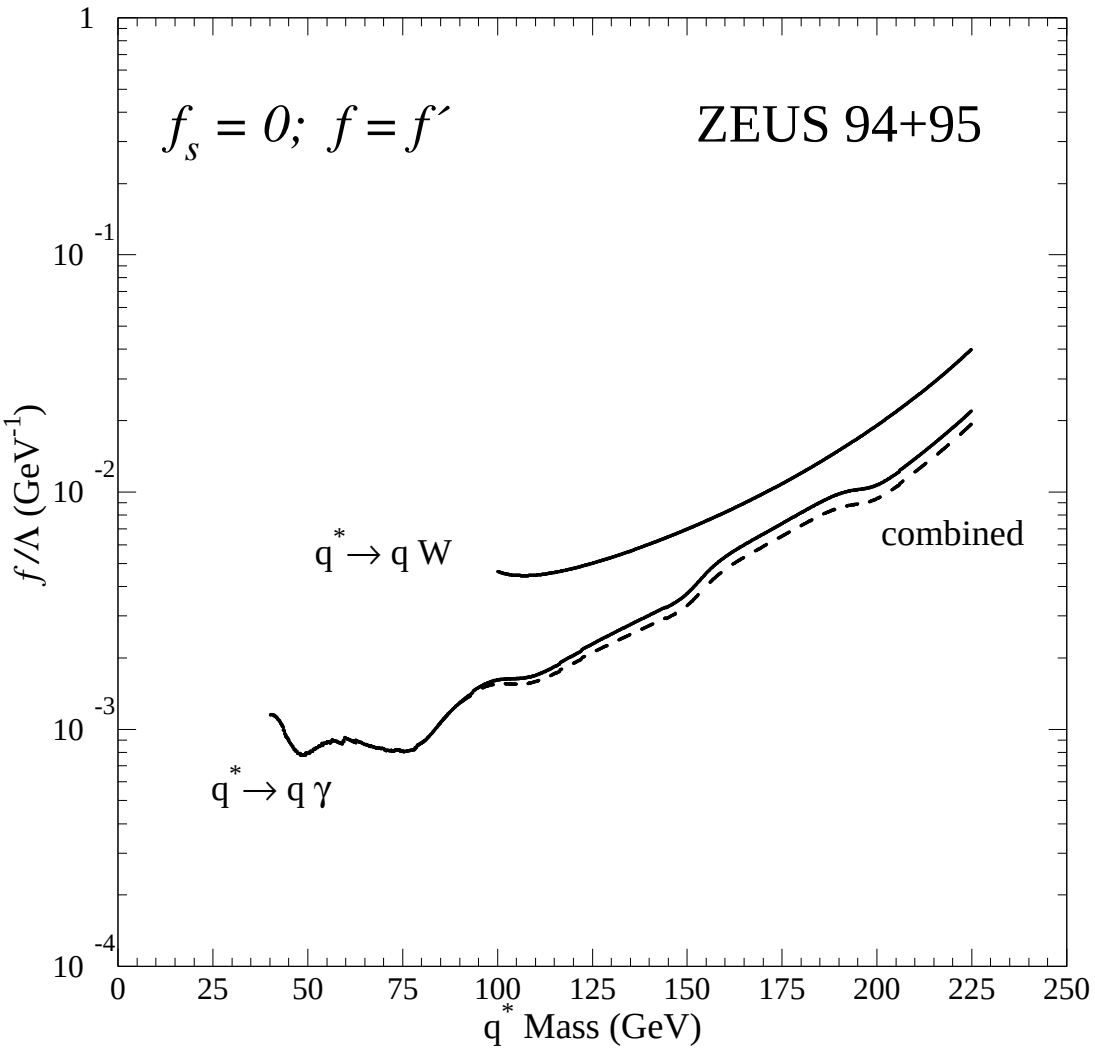

Figure 11: Upper limits at the 95% confidence level on the coupling f/Λ as a function of mass for the excited quark channels assuming $f_s = 0$ (no strong coupling) and $f = f'$. The dashed line is the combined limit from both decay modes.